Integrated stratigraphy of the Oligocene pelagic sequence in the Umbria-Marche basin (northeastern Apennines, Italy): A potential Global Stratotype Section and Point (GSSP) for the Rupelian/Chattian boundary

Rodolfo Coccioni[†]
Andrea Marsili
Istituto di Geologia e Centro di Geobiologia dell'Università degli Studi "Carlo Bo," Campus Scientifico, Località Crocicchia, 61029 Urbino, Italy

Alessandro Montanari
Osservatorio Geologico di Coldigioco, 62020 Frontale di Apiro, Italy
Department of Geology, Carleton College, Northfield, Minnesota 55057, USA

Adriana Bellanca
Rodolfo Neri
Dipartimento di Chimica e Fisica della Terra ed Applicazioni alle Georisorse e ai Rischi Naturali (CFTA), Via Archirafi 36, 90123 Palermo, Italy

David M. Bice
Department of Geosciences, the Pennsylvania State University, University Park, Pennsylvania 16802, USA
Osservatorio Geologico di Coldigioco, 62020 Frontale di Apiro, Italy

Henk Brinkhuis
Laboratory of Palaeobotany and Palynology, Utrecht University, Budapestaan 4, 3584 CD Utrecht, The Netherlands

Nathan Church
Alison Macalady
Aaron McDaniel
Department of Geology, Carleton College, Northfield, Minnesota 55057, USA
Osservatorio Geologico di Coldigioco, 62020 Frontale di Apiro, Italy

Alain Deino
Berkeley Geochronology Center, 2453 Ridge Road, Berkeley, California 94709, USA

Fabrizio Lirer
Mario Sprovieri
Istituto Ambiente Marino Costiero (IAMC)–CNR, Calata Porta di Massa, Interno Porto di Napoli, 80123 Napoli, Italy

Patrizia Maiorano
Dipartimento di Geologia e Geofisica dell'Università degli Studi di Bari, Via Orabona 4, 70125 Bari, Italy

Simonetta Monechi
Dipartimento di Scienze della Terra dell'Università degli Studi di Firenze, Via La Pira 4, 50121 Firenze, Italy

Claudio Nini
Ente Nazionale Idrocarburi (ENI) S.p.A., Exploration and Production Division, Via Emilia 1, 20097 San Donato Milanese, Italy

Marisa Nocchi
Dipartimento di Scienze della Terra dell'Università, Piazza Università 1, 06100 Perugia, Italy

Jörg Pross
Institut für Geowissenschaften, Johann Wolfgang Goethe–Universität Frankfurt, Senckenberganlage 32-34, D-60054 Frankfurt, Germany

[†]E-mail: cron@info-net.it

GSA Bulletin; March/April 2008; v. 120; no. 3/4; p. 487–511; doi: 10.1130/B25988.1; 17 figures; 4 tables.

Pierre Rochette
Université d'Aix Marseille 3, UMR CNRS 6635, CEREGE Europole de l'Arbois BP80 13545 Aix en Provence Cedex 4, France

Leonardo Sagnotti
Istituto Nazionale di Geofisica e Vulcanologia, Via di Vigna Murata 605, 00143 Roma, Italy

Fabio Tateo
Istituto di Geoscienze e Georisorse-CNR, c/o Dipartimento di Geologia, Paleontologia e Geofisica, Via Giotto 1, 35137 Padova, Italy

Yannick Touchard
Université d'Aix Marseille 3, UMR CNRS 6635, CEREGE Europole de l'Arbois BP80 13545 Aix en Provence Cedex 4, France

Stefaan Van Simaeys
Historical Geology, University of Leuven, Redingenstraat 16, B-3000 Leuven, Belgium

Graham L. Williams
Geological Survey of Canada, Bedford Institute of Oceanography, PO Box 1006, Dartmouth, Nova Scotia, B2Y 4A2, Canada

ABSTRACT

The Oligocene represents an important time period from a wide range of perspectives and includes significant climatic and eustatic variations. The pelagic succession of the Umbria-Marche Apennines (central Italy) includes a complete and continuous sequence of marly limestones and marls, with volcaniclastic layers that enable us to construct an integrated stratigraphic framework for this time period. We present here a synthesis of detailed biostratigraphic, magnetostratigraphic, and chemostratigraphic studies, along with geochronologic results from several biotite-rich volcaniclastic layers, which provide the means for an accurate and precise radiometric calibration of the Oligocene time scale. From this study, the interpolated ages for the Rupelian/Chattian stage boundary, located in the upper half of Chron 10n at meter level 188 in the Monte Cagnero section, and corresponding to the O4/O5 planktonic foraminiferal zonal boundary, are 28.36 Ma (paleomagnetic interpolation), 28.27 ± 0.1 Ma (direct radioisotopic dating), and 27.99 Ma (astrochronological interpolation). These ages appear to be slightly younger than those reported in recent chronostratigraphic time scale compilations. The Monte Cagnero section is a potential candidate for defining the Chattian Global Stratotype Section and Point (GSSP) and some reliable criteria are here proposed for marking the Rupelian/Chattian boundary according to International Union of Geological Sciences (IUGS) recommendations.

Keywords: Integrated stratigraphy, Oligocene, Rupelian/Chattian boundary, Umbria-Marche Apennines, central Italy.

INTRODUCTION

The Oligocene represents the last epoch of the Paleogene period, which is a critical time in the evolution of the paleoclimate and paleogeography of the world. Previously considered to represent a stable state, it is now viewed as a period bracketed by large and abrupt climate changes including large fluctuations in the Antarctic ice sheet (Zachos et al., 2001) and related eustatic changes (Miller et al., 1991, 2005) that represent an unusual unipolar glacial world. A thorough understanding of the operation of the global climate system during this period requires a precise and accurate chronostratigraphic framework that facilitates reliable correlations from widespread sections and the measurement of time.

In their integrated Cenozoic time scale, Berggren et al. (1985) subdivided the Oligocene series into a lower stage, the Rupelian, and an upper stage, the Chattian (Fig. 1). Their respective historical stratotypes are located in northwestern Belgium, along the River Rupel near Anvers, and in northwestern Germany, near Kassel (Berggren, 1971; Hardenbol and Berggren, 1978; Van Simaeys et al., 2004). The traditional Rupelian/Chattian stage boundary is placed at the base of the benthic foraminiferal *Asterigerinoides guerichi* acme, known as the *Asterigerina* Horizon.

The traditional Rupelian/Chattian boundary coincides with an abrupt return to shallow warm-water conditions and represents a third-order sequence boundary. The Rupelian/Chattian boundary is overlain by transgressive Chattian deposits, which correspond to a distinct warming event. This pulse may correlate with the globally detected Late Oligocene warming event (Pekar et al., 2006), which has an approximate age of 26 Ma. The absence of calcareous plankton events and magnetostratigraphy prevents the correlation of the historical type sections of both stages to the timescale. Moreover, the historical type localities do not represent suitable and continuous sections for the GSSP that comprise the Rupelian/Chattian boundary.

In search of a continuous section across the Rupelian/Chattian to be proposed as GSSP of the Rupelian/Chattian boundary, we formed the Oligocene Integrated Stratigraphy (OLIS) Working Group, which here provides an integrated stratigraphy of the pelagic Scaglia Cinerea Formation in the Umbria-Marche region of central Italy, spanning the uppermost Eocene through the entire Oligocene Series. Three sections—Pieve d'Accinelli, Monte Cagnero, and Contessa—have been identified and studied to check regional correlations and to establish the best section. A critically important aspect of the three sections studied is that they contain datable volcaniclastic layers in a sequence that also accurately records planktonic and benthonic biozones, magnetic reversals, variations in seawater Sr isotopes, and stable isotopic variations. The combination of all these stratigraphic data in an accessible, complete, and continuous section makes the Monte Cagnero site a particularly strong candidate for the GSSP of the Rupelian/Chattian boundary.

Background

Hardenbol and Berggren (1978) placed the Rupelian/Chattian interstage boundary at the top of the planktonic foraminiferal Zone P19 of Blow (1969), which falls approximately in the middle of the calcareous nannofossil Zone NP23 of Martini (1971). This boundary position was thought to have the best chance of falling between the Rupelian and Chattian historical stages as defined in their respective areas. In the Chattian type section at Doberg, near Munde, northwestern Germany, Martini (1971) tentatively recognized nannofossil Zones NP24 and

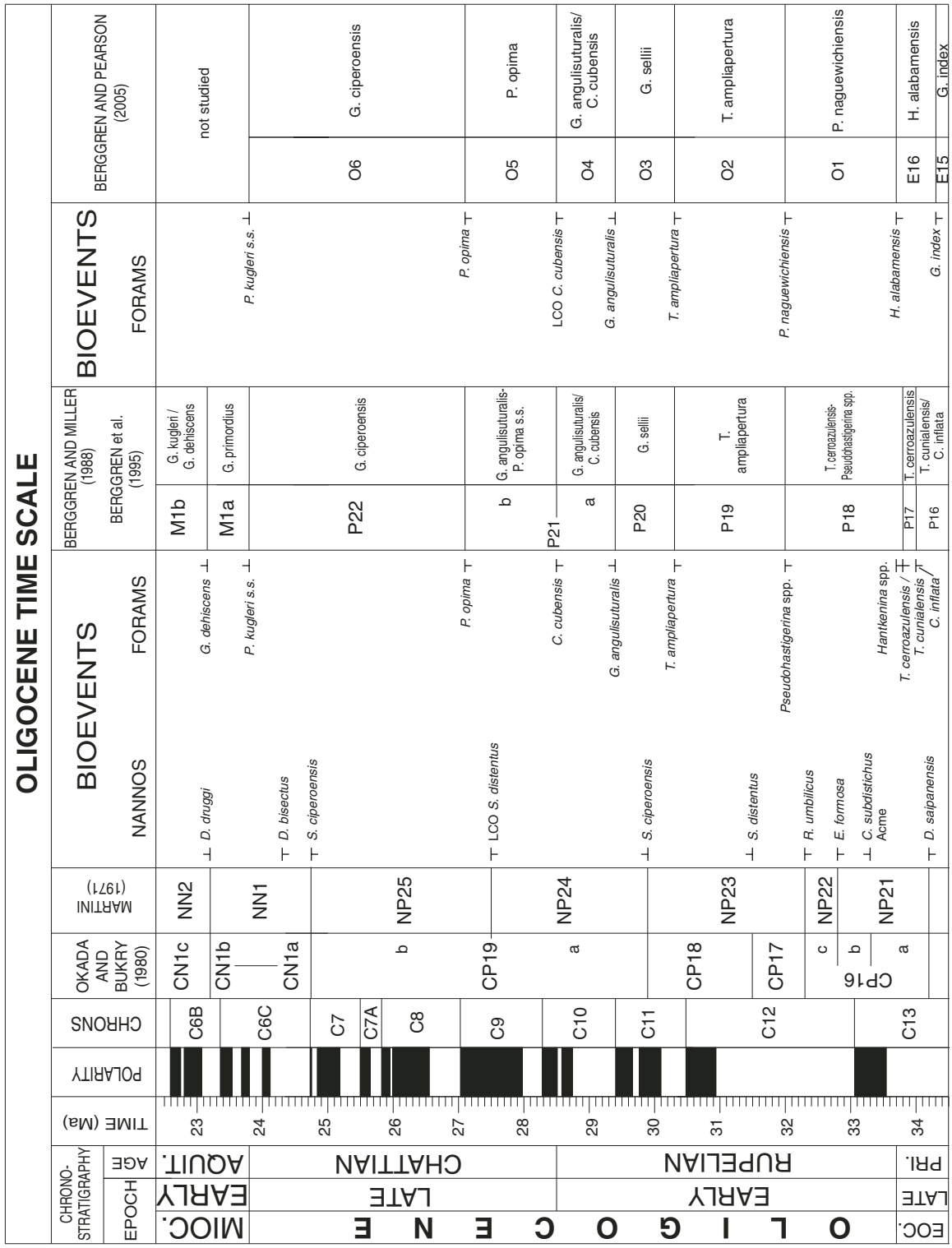

Figure 1. Oligocene time scale (modified after Berggren et al., 1995; Luterbacher et al., 2004; Berggren and Pearson, 2005). LCO—last common occurrence; PRI—Priabonian.

NP25, with the latter zone correlated to the foraminiferal Zone P22 and the lower part of Zone N4 of Blow (1969).

In more recent biostratigraphic, magnetostratigraphic, and chronostratigraphic assessments (e.g., Berggren et al., 1995; Berggren and Pearson, 2005), this interstage boundary was moved stratigraphically higher to coincide with the P21a/P21b zonal boundary of Berggren and Miller (1988) or the O4/O5 zonal boundary of Berggren and Pearson (2005), which is based on the last common occurrences (LCO) of the planktonic foraminifer *Chiloguembelina cubensis*. This event falls in the middle part of Zone NP24 of Martini (1971) and within polarity Chron 10n (Fig. 1). According to Van Simaeys et al. (2004). In the Rupelian/Chattian type section, planktonic foraminifera are rare throughout the neritic upper Rupelian, and the Rupelian/Chattian boundary coincides with the first occurrences (FOs) of the benthic foraminifera *Elphidium subnodosum* and *Protoelphidium roemeri*, which are coeval with the onset of the *Asterigerinoides guerichi* acme, also known as the *Asterigerina* Horizon (Van Simaeys et al., 2004). This bloom goes together with major changes in dinocyst and nannofossil species abundances, and appears to be due to the onset of a shallow, warm-water depositional environment. In terms of dinocyst biostratigraphy, the *Asterigerina* Horizon coincides with the FO of *Artemisiocysta cladodichotoma* and the recurrence of *Pentadinium imaginatum*, falling within the middle of the NP24 nannofossil Zone of Martini (1971). However, due to their endemic nature, the *Asterigerina* Horizon, cannot be calibrated with the international magnetochronologic time scale.

In the Umbria-Marche basin, the Rupelian/Chattian boundary falls within the Scaglia Cinerea Formation based on biostratigraphic correlations (the LCO *Chiloguembelina* spp.) from unit stratotypes in northwest Europe (e.g., Berggren et al., 1995). This unit constitutes the upper part of a thick, largely pelagic carbonate succession, and is characterized by marly limestone, calcareous marl, and marl beds of gray color with some important intercalations of biotite-rich layers. The first integrated stratigraphic study of the Oligocene in the Umbria-Marche pelagic sequence, which included lithostratigraphy, calcareous plankton biostratigraphy, and magnetostratigraphy of the entire Scaglia Cinerea, was carried out by Lowrie et al. (1982) in a quarry exposure (the Contessa Quarry section) at the head of the Contessa Valley, ~3 km west of the medieval city of Gubbio (Figs. 2 and 3). In their study, Lowrie and coworkers reported several biotite-rich layers distributed throughout a stratigraphic interval across the Eocene/Oligocene boundary. These layers were first dated by

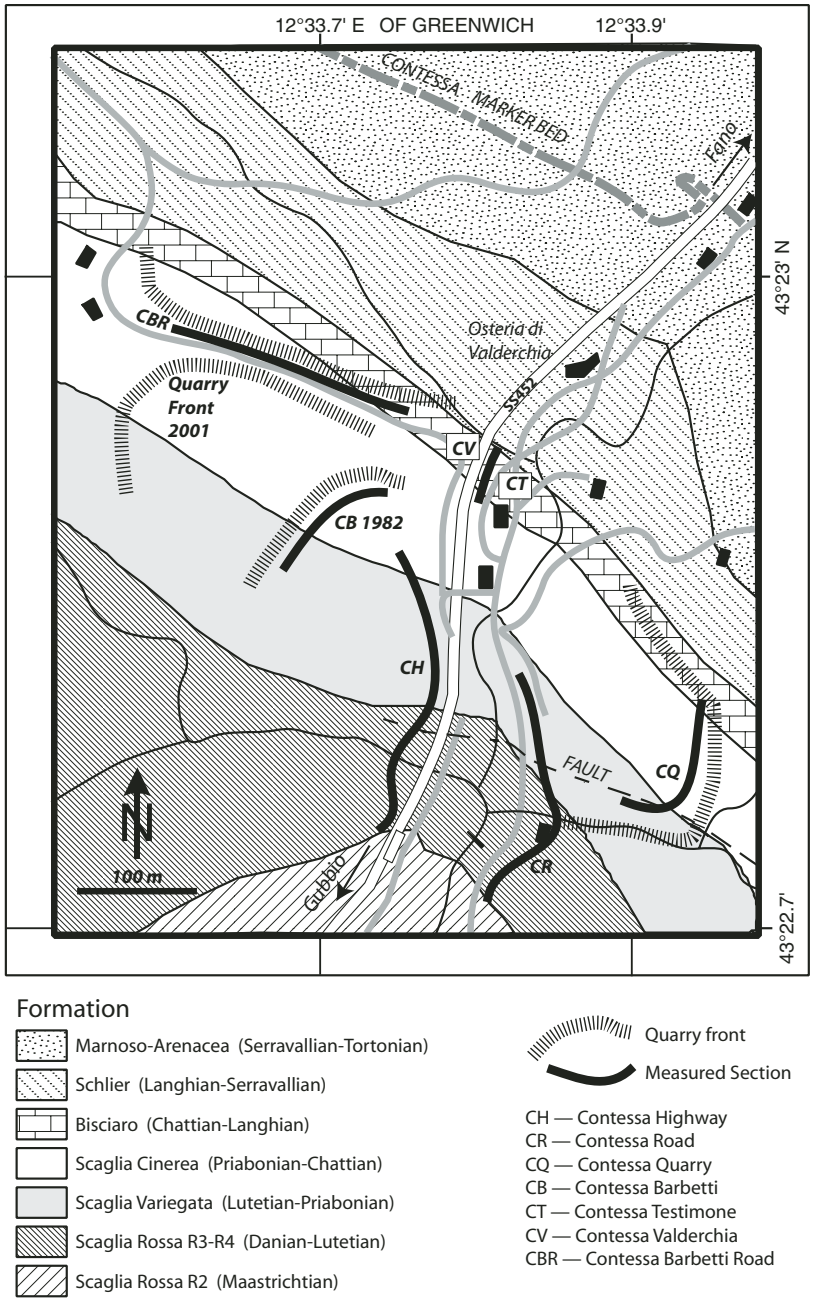

Figure 2. Location map of the Contessa sections (CH, CR, CQ, CB, CT, and CV) and the new Contessa Barbetti Road (CBR) section.

Montanari et al. (1985) along with other similar biotite-rich layers in other sections throughout the Umbria-Marche region. The wealth of radioisotopic dates obtained from this pelagic sequence was instrumental in the calibration of the bio-magnetostratigraphic time scale of the upper Eocene-Oligocene interval (e.g., Berggren et al., 1985, 1995; Harland et al., 1990). However, while additional detailed studies were focused on the stratigraphic intervals containing the Eocene/Oligocene and Oligocene/Miocene boundaries (see Montanari and Koeberl, 2000, and references therein), refinement of the remaining Oligocene of the Umbria-Marche succession (i.e., the interval containing the Rupelian/Chattian boundary) was not pursued following the work of Lowrie et al. (1982) and Montanari et al. (1985), prior to the present Oligocene Integrated Stratigraphy (OLIS) Working Group study. The purpose of the OLIS Working Group was to provide a refined integrated stratigraphy of the Oligocene in the Umbria-Marche

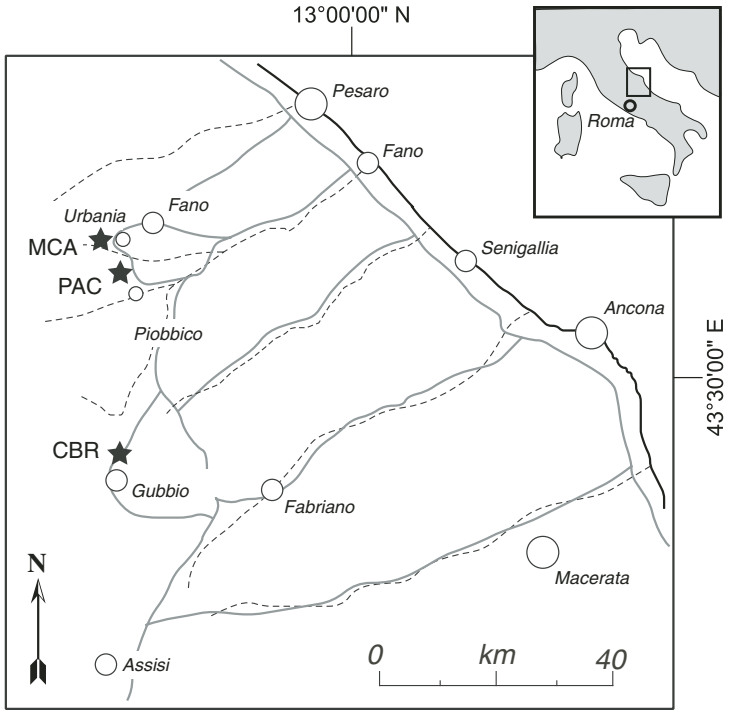

Figure 3. Location map of Contessa Barbetti Road (CBR), Pieve d'Accinelli (PAC), and Monte Cagnero (MCA) sections.

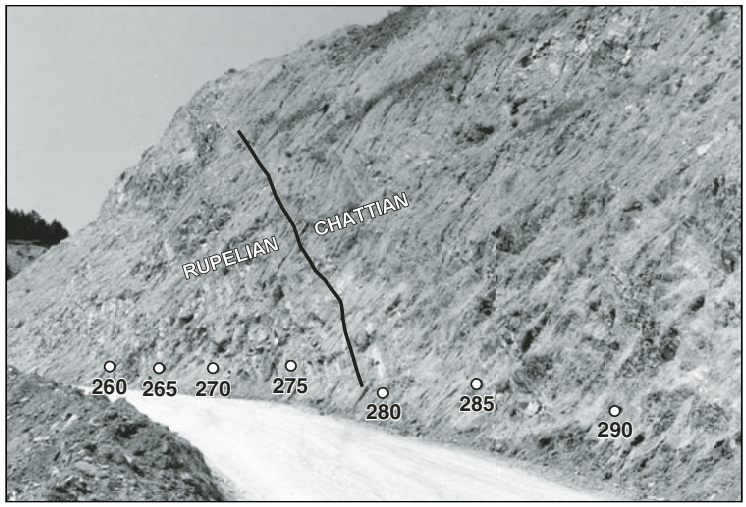

Figure 4. Sampling trajectory of the Contessa Barbetti Road (CBR) section.

succession, especially focusing on the interval across the Rupelian/Chattian boundary.

The three most complete and continuous exposures of this interval in this region (Fig. 3), the Pieve d'Accinelli section (PAC) near Piobbico, the Monte Cagnero (MCA) section near Urbania, and the Contessa Barbetti Road (CBR), the latter a new road cut in the large Barbetti quarries near Gubbio, were chosen for detailed calcareous plankton and dinoflagellate biostratigraphy, magnetostratigraphy, and isotope chemostratigraphy ($\delta^{18}O$, $\delta^{13}C$, and $^{87}Sr/^{86}Sr$). Biotite-rich layers in the Contessa Barbetti Road and Contessa Quarry (CQ) sections at Contessa and the Monte Cagnero section were re-dated with the $^{40}Ar/^{39}Ar$ technique to verify the reliability of geochronologic tie points for the calibration of the Oligocene time scale. In fact, recent Oligocene numerical time scales (e.g., Berggren et al., 1985, 1995; Harland et al., 1990; Cande and Kent, 1992, 1995) are calibrated using just a few radioisotopic age tie points, two of which are represented by these Umbria-Marche biotite-rich, volcaniclastic layers.

Biotite from the lower layer, located in the upper Chron 12r of the Contessa Quarry section (Lowrie et al., 1982), yielded a mean K/Ar age, from two replicates, of 32.0 ± 0.7 Ma (Montanari et al., 1985). The same authors also dated, with the K/Ar method, a biotite separate from a similar layer found in the Monte Cagnero section, obtaining an age of 31.7 ± 0.6 Ma. The upper biotite layer, which was placed by Montanari et al. (1985) at the base of Chron 9n in the Contessa Quarry section, using the magnetostratigraphic work of Lowrie et al. (1982), yielded a mean K/Ar age, from two replicate dates, of 28.1 ± 0.4 Ma, and a Rb/Sr age of 27.8 ± 0.2 Ma. While the $^{40}Ar/^{39}Ar$ dating of lower biotite layers yielded results consistent with previous K/Ar dates, re-dating of the upper layer revealed an inconsistent radioisotopic behavior, which will be discussed below.

MATERIALS AND METHODS

Planktonic Foraminifera

The three studied sections were sampled for micropaleontological analysis with different sampling density: 61 samples were collected at a mean interval of 1 m in the Contessa Barbetti Road section (Figs. 4 and 5), 103 samples were collected at a mean interval of 0.5 m in the Pieve d'Accinelli section (Figs. 6 and 7), and 161 samples were collected at a mean interval of 0.5 m in the Monte Cagnero section (Figs. 8 and 9). The planktonic foraminiferal analysis is based on 61 samples for the Contessa Barbetti Road section, 103 for the Pieve d'Accinelli section, and 81 for the Monte Cagnero section. Samples were prepared using standard micropaleontological techniques for the marly and calcareous-marly lithologies. They were disaggregated with Desogen and rinsed through a sieve with 63 µm mesh, with the exception of the thin interval around the early and late Oligocene boundary, where a 32 µm mesh sieve was used. The washed residues were soaked again in Desogen for several hours and then immersed in an ultrasonic bath for a few minutes. The final washed residue was split in two fractions, a finer one between 63 µm and 150 µm, and a coarser one >150 µm.

Following the taxonomic criteria of Bolli and Saunders (1985), Spezzaferri (1994, 1998), and Berggren and Pearson (2005), we based our biozonal definitions according to Berggren et al. (1995), updated by Berggren and Pearson (2005). In agreement with Berggren and Pearson (2005), we used the last occurrence (LO, which is defined as the highest occurrence by these

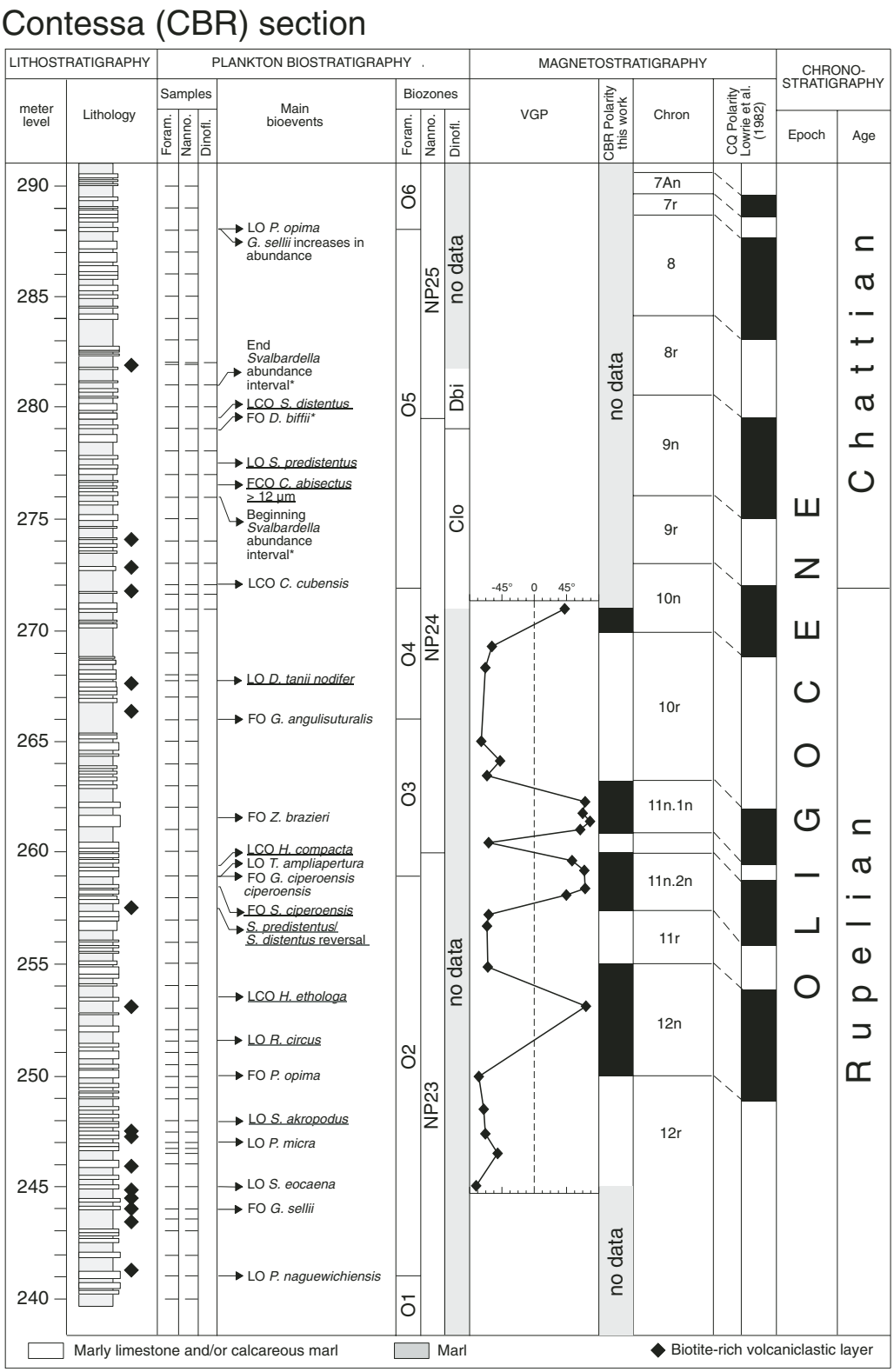

Figure 5. Integrated stratigraphy of the Contessa Barbetti Road (CBR) section with magnetostratigraphic interpretation. Paleomagnetic data are expressed as virtual geomagnetic pole (VGP) latitudes computed after bringing the mean declination to the north-south direction to correct for tectonic rotation. Correlation to the magnetic polarity timescale is quite straightforward using the longer Lowrie et al. (1982) polarity record and the available paleontological constraints. Underline—calcareous nannofossil events; asterisk—dinoflagellate cyst events; unmarked—planktonic foraminiferal events. Biozones after Berggren and Pearson (2005) for planktonic foraminifera; Martini (1971) for calcareous nannofossil; and Brinkhuis and Biffi (1993) for dinoflagellate cysts.

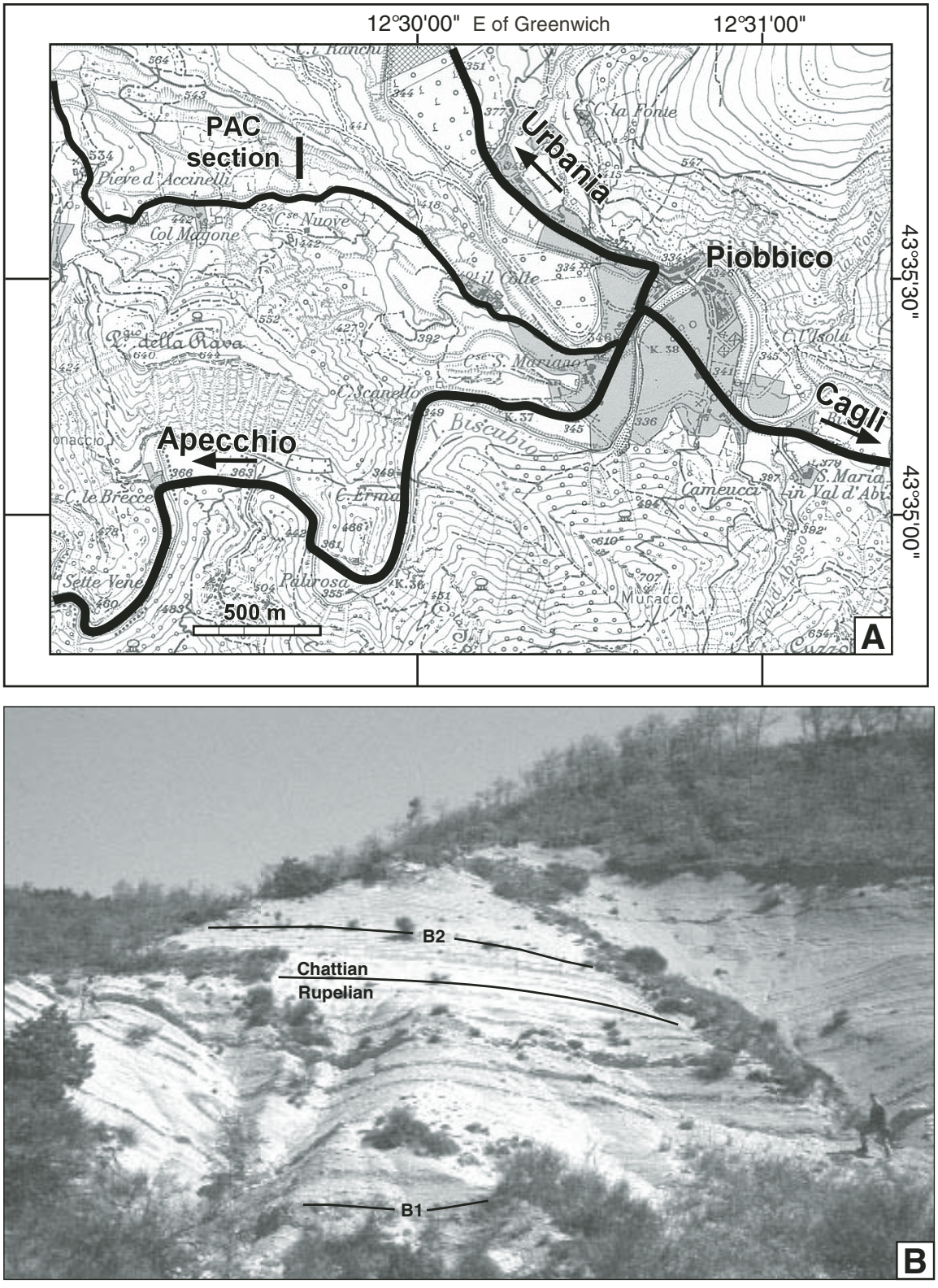

Figure 6. Sampling trajectory of the Pieve d'Accinelli (PAC) section (A) and the PAC section exposure (B). B1 and B2 are two distinct, biotite-rich volcaniclastic layers (see Fig. 7).

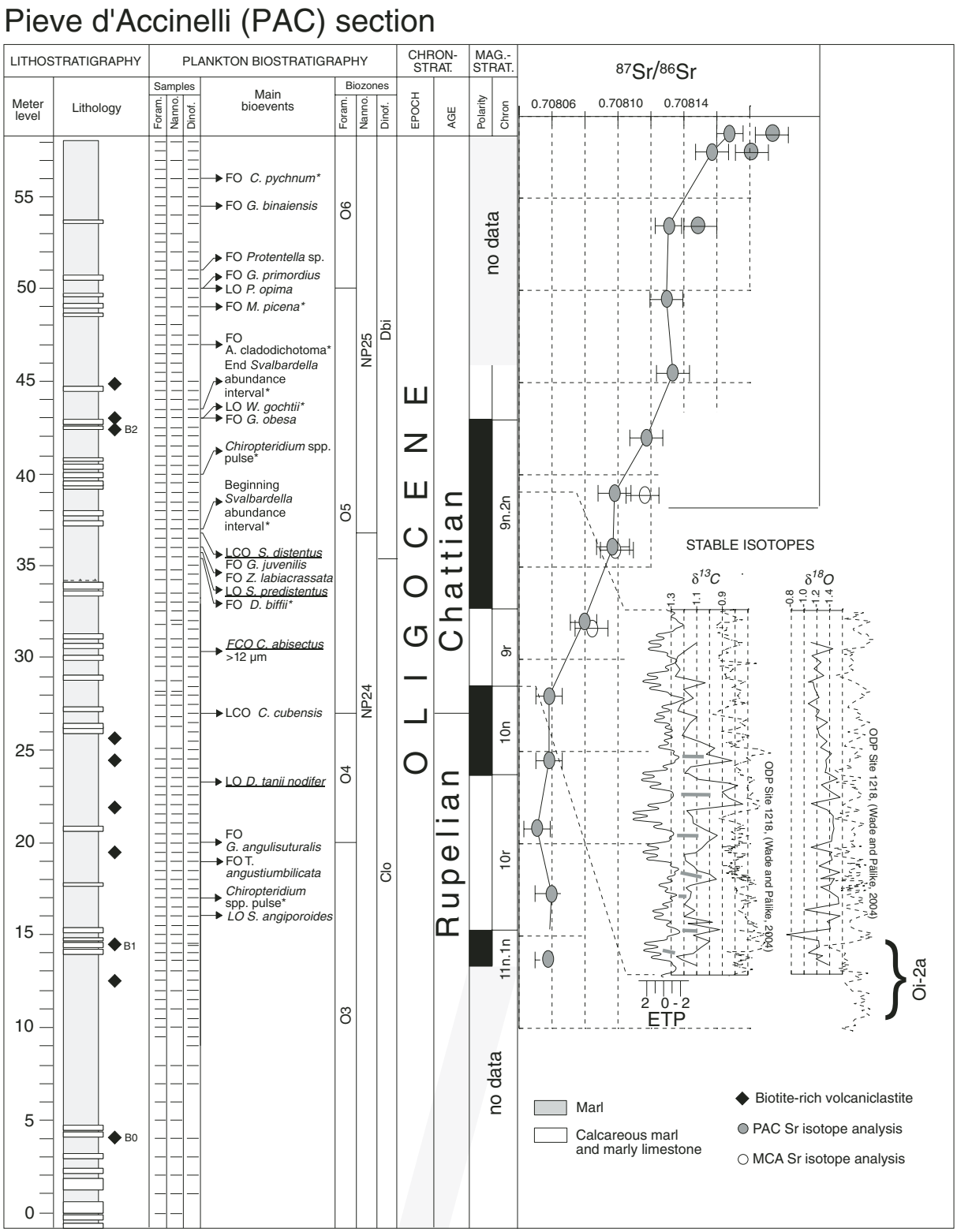

Figure 7. Integrated stratigraphy of the Pieve d'Accinelli (PAC) section. Underline—calcareous nannofossil events; asterisk—dinoflagellate cyst events; unmarked—planktonic foraminiferal events. Biozones as in Figure 5. Sr data are mainly from the PAC section: a few Monte Cagnero (MCA) Sr data are shown, correlated on the basis of magnetostratigraphy and biostratigraphy. High-resolution stable isotope data for earliest Chattian are shown, with an expanded scale, compared to the composite astronomical curve eccentricity, tilt, and precession (ETP) (Laskar et al., 2004) and stable isotope data from Ocean Drilling Program (ODP) Site 1218 (Wade and Pälike, 2004), with an offset scale to aid comparison. The ETP and ODP curves were correlated to the PAC section on the basis of magnetostratigraphy. Gray lines show connection between $\delta^{13}C$ maxima and ETP minima associated with the ~100 k.y. eccentricity.

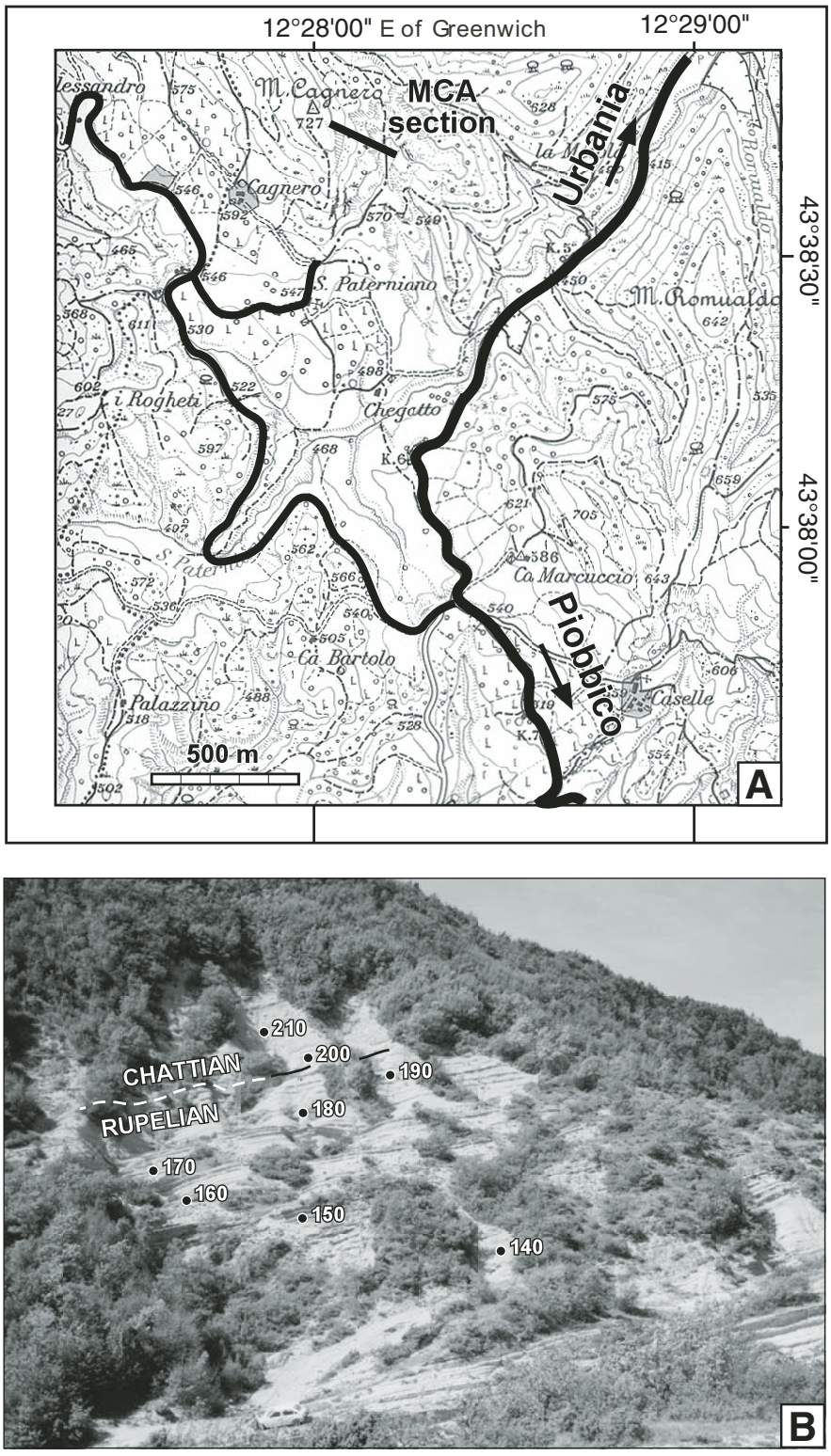

Figure 8. (A) Location of the Monte Cagnero (MCA) section. (B) Sampling trajectory of the MCA section.

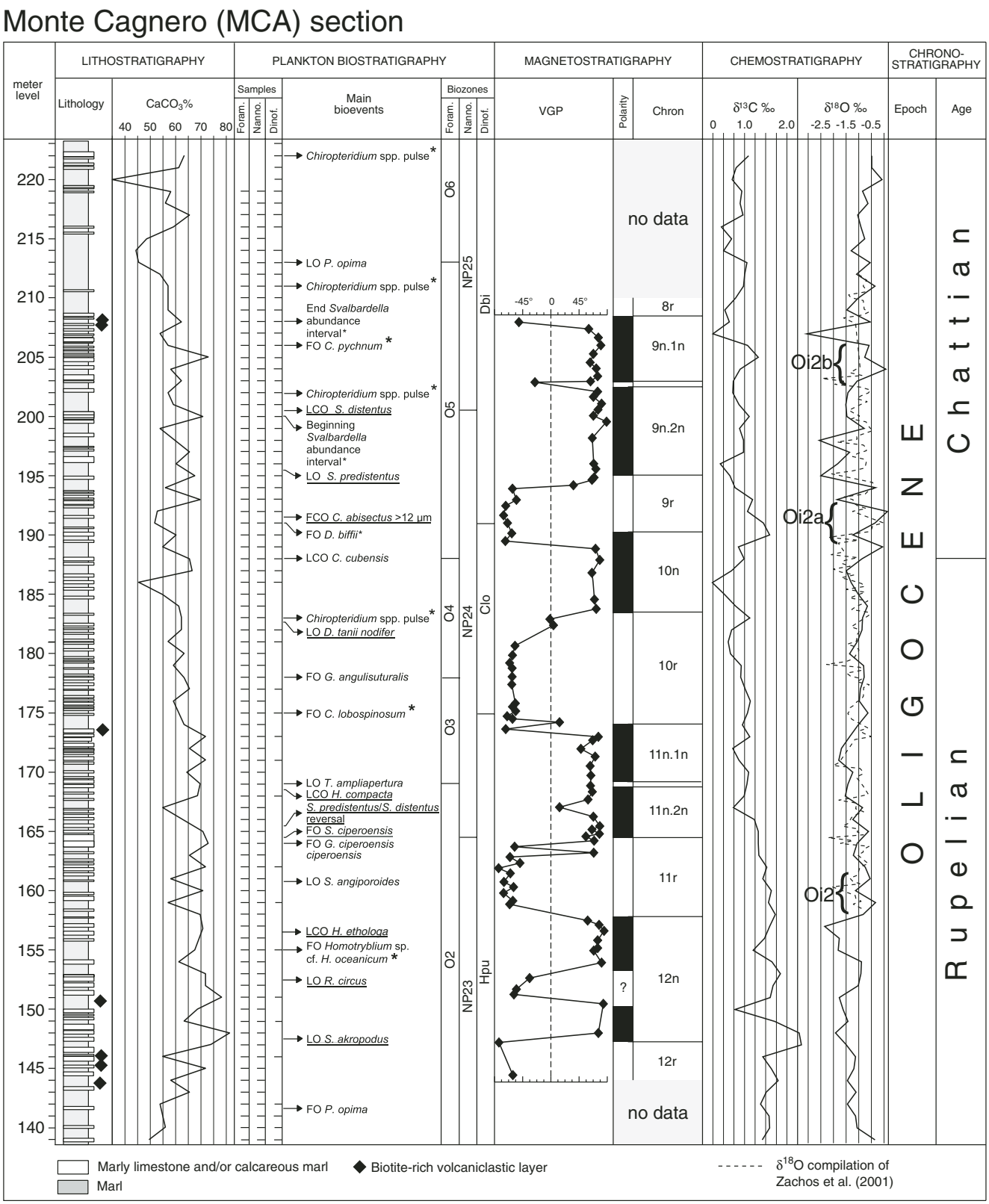

Figure 9. Integrated stratigraphy of the Monte Cagnero (MCA) section with magnetostratigraphic interpretation. Paleomagnetic data are expressed as virtual geomagnetic pole (VGP) latitudes computed after bringing the mean declination to the north-south direction to correct for tectonic rotation. Composite $\delta^{18}O$ record from Zachos et al. (2001) is shown for comparison with the MCA data; glacial events Oi-2, Oi-2a, and Oi-2b from Wade and Pälike (2004). Underline—calcareous nannofossil events; asterisk—dinoflagellate cyst events; unmarked—planktonic foraminiferal events. Biozones as in Figure 5.

authors) of *Pseudohastigerina naguewichiensis* to recognize the O1/O2 zonal boundary, the LO of *Turborotalia ampliapertura* to denote the O2/O3 zonal boundary, the FO (which is defined as the lowest occurrence by these) of *Globigerina angulisuturalis* to mark the O3/O4 zonal boundary, and the LO of *Paragloborotalia opima* to place the O5/O6 zonal boundary (Fig. 1).

The LO of *Chiloguembelina cubensis,* which marks the boundary between Subzones P21a and P21b of Berggren and Miller (1988) and Berggren et al. (1995), is the worldwide criterion for the recognition of the Rupelian/Chattian boundary (see also Luterbacher et al., 2004). Reported sporadic occurrences of *C. cubensis* throughout the upper Oligocene, in particular from western tropical Pacific (Ontong Java Plateau) and western subtropical North Atlantic Holes (Little Bahama Bank; see Leckie et al., 1993), have led Berggren and Pearson (2005) to modify the criterion for the upper limit of Subzone P21a to LCO of *C. cubensis* rather than its LO and to elevate the lower and upper parts of Zone P21 to the rank of zones (as Zones O4 and O5, respectively) (see Fig. 1).

Calcareous Nannofossils

The calcareous nannofossil analyses were performed on 61, 90, and 81 samples from the Contessa Barbetti Road, Pieve d'Accinelli, and Monte Cagnero sections, respectively (Figs. 5, 7, and 9). Light microscope techniques at 1000× magnification were used for examination of smear slides prepared using standard methods. Assemblage preservation varies from poor to moderate with etching (E-2 and E-3) and overgrowth (O-2 and O-3) following Roth and Thierstein (1972) and modified by Roth (1983). Quantitative analyses have been performed to recognize FOs and LOs, as well as first common occurrence (FCO) and LCO. FCO and LCO are defined as the beginning and the end of a continuous and consistent pattern. Abundances of common species such as *Cyclicargolithus abisectus, C. floridanus*, and reticulofenestrids were obtained after counting 300 specimens. In addition, counting of 100 sphenolithids was performed on this genus; helicolithids and discoasterids are often rare in the assemblages and their abundance patterns were collected counting index species in an area of 150 views. Abundance patterns obtained in the three studied sections have been presented in a separate paper (Maiorano and Monechi, 2006).

The calcareous nannofossil standard zonation of Martini (1971) and Okada and Bukry (1980) are widely adopted for low and middle latitude Oligocene biostratigraphic studies. Unfortunately, the biostratigraphic resolution of the standard schemes in this time interval is considerably low. More recent works in the equatorial Indian Ocean (Fornaciari et al., 1990), in the northeastern Atlantic Ocean (de Kaenel and Villa, 1996), and in a few Mediterranean land sections (Catanzariti et al., 1997) have led to an improvement of the low-resolution standard schemes. Quantitative analyses performed in this study on the Contessa Barbetti Road, Pieve d'Accinelli, and Monte Cagnero sections, allow us to test the biostratigraphic consistency of the conventional events in standard zonations as well as to propose new bioevents, improving the Oligocene biostratigraphic resolution within the Mediterranean region.

The calcareous nannofossil zonal boundaries through NP23–NP25 are traced according to the standard zonation of Martini (1971) with slight modification for the definition of the NP24/NP25 boundary, for which the LCO of *Sphenolithus distentus* is used here instead of its LO. In fact, in all the studied sections, *Sphenolithus distentus* is very rare and scattered during its final range (Maiorano and Monechi, 2006), while the sharp decrease in abundance of the species enables an easy detection of the LCO of *S. distentus,* which seems to be a more reliable biostratigraphic signal than the LO. The LCO of *S. distentus* can be compared to the "distinct drop in abundance" of the species recorded in the equatorial Indian Ocean (Fornaciari et al., 1990) and to the "final decline in abundance" observed in the Atlantic and Indian Oceans (Olafsson and Villa, 1992) and therefore can be recognized worldwide. We do not rely on the LO of *S. predistentus* as an alternative event for the identification of the NP24/25 zonal boundary, as suggested by Fornaciari et al. (1990) and de Kaenel and Villa (1996), since the species is discontinuously present during the final distribution (Maiorano and Monechi, 2006). In addition to a few standard and well-known bioevents represented by the FO of *S. ciperoensis* and the LO of *S. predistentus*, several secondary events were recognized allowing a higher biostratigraphic resolution of the NP23 and NP24 Zones. These events are: the LO of *S. akropodus,* the LO of *Reticulofenestra circus*, the LCO of *Helicosphaera ethologa* in Zone NP23 and the reversal in abundance between *S. predistentus* and *S. distentus,* the LCO of *H compacta,* the LO of *Discoaster tanii nodifer*, and the FCO of *Cyclicargolithus abisectus* >12 µm in the NP24 Zone.

Most of the secondary events proved to have a supraregional biostratigraphic meaning since they were reported also from the Atlantic Ocean (de Kaenel and Villa, 1996). The FCO of *C. abisectus* >12 µm seems to be a reliable event also in the eastern tropical Atlantic Site 667A and the reversal in abundance between *S. predistentus* and *S. distentus* can be inferred from several abundance patterns available from the Atlantic and Indian Oceans (Fornaciari et al., 1990; Olafsson and Villa, 1992).

Dinoflagellate Cysts

Dinoflagellate cyst (dinocysts) analysis is based on 12 samples from the Contessa Barbetti Road section, 101 samples from the Pieve d'Accinelli section, and 54 samples from the Monte Cagnero section (Figs. 5, 7, and 9). Samples were processed using standard palynological techniques at Laboratory of Palaeobotany and Palynology (LPP) Utrecht University (Pieve d'Accinelli), Tübingen University (Contessa Barbetti Road), and the Geological Survey of Canada (Monte Cagnero). The slides were analyzed qualitatively and quantitatively following the methodology of Brinkhuis and Biffi (1993). The adopted dinocyst taxonomy is that of Williams et al. (1998). Materials are stored either in the collection of Utrecht University (Pieve d'Accinelli and Monte Cagnero) or Tübingen University (Contessa Barbetti Road). The present paper reports on selected, stratigraphically important, dinocyst events.

Magnetostratigraphy

Oriented core samples (2.5 cm diameter) were collected and analyzed at one-meter intervals through a short interval of the Contessa Barbetti Road section, from 245 m to 271.05 m, to correlate this new outcrop with the original Contessa Quarry section of Lowrie et al. (1982), which is located on the opposite (east) side of the quarry across the Contessa Highway. Paleomagnetic measurements have been carried out at the National Institute of Geophysics and Volcanology (INGV) in Rome and at Le Centre Européen de Recherche et d'Enseignement des Géosciences de l'Environnement (CEREGE) Laboratory in Marseille using either a 2G cryogenic magnetometer or an AGICO JR-5A spinner magnetometer, within magnetically shielded rooms. Because Lowrie et al. (1982) found that natural remanent magnetization (NRM) of the Scaglia Cinerea was carried by high-stability, fine-grained magnetite, with little secondary magnetization easily removed by alternating field (AF) treatment, only this technique was used to isolate the characteristic remanent (ChRM) direction. In this study, we used AF demagnetization steps of 0, 5, 10, 15, 20, 30, 40, 50, 60, 80, and 100 mT, at which point the intensity decayed within the noise level for most of the samples. To evaluate the additional possible presence of high-coercivity magnetic minerals, we also measured the isothermal remanent magnetization

(IRM) acquired in pulse fields of 0.9 T and –0.3 T, in sequence, that allowed the computation of the dimensionless S-ratio (IRM-0.3T/IRM0.9T), which is a coercivity-dependent parameter.

Fifteen oriented samples (PAC/97 collection) covering the lower 12 m of the Pieve d'Accinelli section (Fig. 6 and 7) were analyzed at INGV and CEREGE. Due to strong fracturing and intense weathering of the lower part of the section, only NRM was measured through stepwise AF demagnetization. In addition to these samples, 45 core samples, with a 25 mm diameter, were drilled in at the Geological Observatory of Coldigioco from oriented hand samples, which were collected at an average stratigraphic spacing of 60 cm, covering the section from 14 m up to 46 m (Fig. 7). In a second sampling campaign (PAC/98), 20 additional samples were collected using a portable, gasoline-powered drill with a 25-mm–diameter diamond bit. These additional samples were analyzed to improve the magnetostratigraphic resolution across three magnetic polarity reversals between 27 m and 41 m of the section. A variety of rock magnetic analyses were carried out at the University of Minnesota's Institute of Rock Magnetism. From the PAC/97 collection, a total of 68 specimens were analyzed using a spinner magnetometer to find the NRM. Twenty-three specimens were progressively demagnetized using alternating fields of 10, 20, 30, 45, and 60 mT, at which point the magnetization was often too weak for the magnetometer to give accurate readings. Several specimens were demagnetized in fields of 80 and 100 mT. Eight specimens were thermally demagnetized at steps of 100, 200, 300, 350, and 400 °C, and for two specimens, 450 °C. The remaining specimens were simply heated to 300 °C to remove overprinting and were then analyzed in the spinner. The samples PAC/98 were also subjected to a similar demagnetization procedure, but they were measured in a cryogenic magnetometer instead of the spinner.

In the Monte Cagnero section (Figs. 8 and 9), we collected 91 oriented cores, spanning 64 m of stratigraphic sequence, from 144 m to 209 m. The samples were analyzed at the INGV and CEREGE laboratories with the same methodology used for the Contessa Barbetti Road samples. However, in the Monte Cagnero section, we first carried out a pilot study on ten specimens using the same AF stepwise demagnetization procedure employed for the Contessa Barbetti Road samples; then all the remaining samples were demagnetized in steps of 0, 5, 10, 20, 30, 40, and 60 mT, at which level the remanence decayed within the noise level. Demagnetization data were treated in the same way as the Contessa Barbetti Road samples.

Mineralogy

Eighty-two samples from the Pieve d'Accinelli section (Fig. 7) were analyzed semiquantitatively by X-ray diffraction (XRD). Seven samples were examined with a petrographic microscope to verify the occurrence of volcaniclastic minerals.

Oxygen, Carbon, and Strontium Isotopes

Bulk-rock samples were collected across a 34 m interval in the Pieve d'Accinelli section at 90 cm intervals, from 114.79 m up to 137.73 m, covering the upper part of P20 Zone, the entire P21a Zone, and most of P21b Zone. Through an 8 m interval across the P21a/P21b boundary (i.e., the Rupelian/Chattian boundary), samples were collected every 15 cm (Fig. 7). Samples were analyzed for carbon and oxygen isotope ratios at the Paleoclimatology Laboratory of the University of California at Santa Cruz. Bulk samples were dried in a 50 °C oven overnight and then crushed into a homogeneous powder. Next, they were dissolved in a common 90 °C H_2PO_4 acid bath linked to a mass spectrometer, which analyzed the CO_2 resulting from this reaction. Percent carbonate data were generated by measuring the gas pressure of CO_2 from each sample as it passed through the transducer of the mass spectrometer. The sample's CO_2 pressure and mass were plotted against the pressure and mass of an internal standard (Carrara marble) that is assumed to be 100% carbonate. All isotope results reported in this paper are in parts per mil relative to the Peedee Belemnite (PDB) standard. Internal error was calculated by running another standard, Carrara marble. This error was less than 0.13‰ for oxygen, and 0.04‰ for carbon isotope results.

In the Monte Cagnero section, a total of 98 bulk-rock samples were collected at 1 m intervals (Fig. 9) and analyzed at the Isotope Laboratory of the University of Parma. Bulk samples were roasted for 40 min at 430 °C in high-vacuum glass tubes and then dissolved in 100% phosphoric acid at 25 °C under high vacuum for 12 h. The CO_2 was cryogenically separated from other gases and measured with a Finnigan Delta S mass spectrometer. All isotopic results are expressed in ‰ units and reported against the Vienna Peedee Belemnite (VPDB)-1 standard. The reproducibility for the isotopic determinations was ±0.1‰ for $\delta^{18}O$ and ±0.07‰ for $\delta^{13}C$. Carbonate percentages of the Monte Cagnero samples were determined by means of a conventional, gas-volumetric methodology (Husselmann, 1966), and plotted against carbon and oxygen isotope results in Figure 9.

For analysis of Sr isotopes, 14 ~2 cm^3 bulk samples were collected in the Pieve d'Accinelli section approximately every 4 m, starting at 13.5 m up section to 58 m (Fig. 7), and three additional samples were collected in the Monte Cagnero section at 4 m intervals, starting from a level that stratigraphically correlates with Pieve d'Accinelli 31.5 m on the basis of biomagnetostratigraphy and magnetostratigraphy (Fig. 9). The strontium isotopic compositions of these samples, ranging from 17.3 to 21.2 mg, were analyzed at the Berkeley Institute for Isotope Geochemistry, using sample preparation and analytical procedures similar to those described by DePaolo and Ingram (1985), Capo and DePaolo (1988), and Montanari et al. (1991, 1997a, 1997b), who analyzed bulk-rock samples from upper Eocene to upper Miocene pelagic limestones and marls of the Umbria-Marche succession.

Geochronology

Biotite and plagioclase crystals were analyzed from the Contessa Barbetti Road and Monte Cagnero sections by the laser, incremental-heating $^{40}Ar/^{39}Ar$ technique at the Berkeley Geochronology Center. The biotite flakes were separated from the enclosing rocks following the methods of Montanari et al. (1985). In short, wet sieving and isomagnetic separation techniques were applied to avoid the use of acids to break down the bulk rock, which might have caused leaching of potassium from the mineral, and possible nonproportional loss of argon. Impurities were eliminated by hand picking and/or further wet sieving after having crushed the biotite separates with a cylinder ball mill. Plagioclase grains were separated from the >63 µm washed residues using a graded column of heavy chromium metatungstenate liquid. The Fish Canyon Tuff sanidine was used as the neutron-flux monitor mineral, with an age of 27.84 Ma. For more details about the $^{40}Ar/^{39}Ar$ dating methodology, see Deino et al. (1997) and references therein.

INTEGRATED STRATIGRAPHY OF THE STUDIED SECTIONS

Lithostratigraphy

The bedding of the Scaglia Cinerea Formation is characterized, in all the studied sections, by a fairly regular alternation of light-gray to blue-gray marly limestone, calcareous marl and marl layers, 10–20 cm thick, with a fissile appearance imparted by closely spaced, bedding-parallel, pressure-solution surfaces. In addition, biotite-rich levels are found in clusters through discrete stratigraphic intervals. Biogenic calcite is the most abundant mineral (~60%), with minor amounts of detrital sheet silicates, and quartz.

The Contessa Barbetti Road section was measured carefully, marked at every meter starting from the base of the Bisciaro Formation down section, following the stratimetric system of the original Contessa Quarry section of Lowrie et al. (1982) (Fig. 5). When Montanari et al. (1985) relocated the dated biotite levels originally found by Lowrie et al. (1982) by remeasuring the Contessa Quarry section through the Scaglia Cinerea down from the easily recognizable base of the Bisciaro Formation at 306 m, they may have introduced stratigraphic errors on the order of a few meters. Further studies in the Contessa Quarry (CQ) and Contessa Barbetti (CB) sections (Fig. 2) were made impossible, in the following years, due to the quarrying activity of the Barbetti Cement Company. The Contessa Quarry face has been mostly covered by debris, whereas the Contessa Barbetti quarry front has been mined back into the mountain for a few hundred meters. Nevertheless, in recent years the Barbetti Cement Company constructed a new truck road on the east side of the Contessa Barbetti quarry, thus creating a new, continuous exposure throughout most of the Oligocene Scaglia Cinerea and the overlying Miocene Bisciaro formations. This new exposure, called the Contessa Barbetti Road (CBR) section (Figs. 2, 4, and 5) offered us the possibility to recalibrate the sedimentary succession studied by Lowrie et al. (1982), and dated by Montanari et al. (1985). In the 51-m–thick Contessa Barbetti Road section (Fig. 5), the interval between 244 m and 249 m has a more marly (soft) appearance, and exhibits a faint reddish tinge. Biotite-rich levels are found in clusters through two discrete, stratigraphic intervals. The lower interval stretches from 241 m to 248 m, while the second cluster is found between 266 and 274 m. The most abundant biotite level in the lower cluster is found at meter level 247.2, and it corresponds to the level CQ-GAR-247 dated by Montanari et al. (1985). In the second cluster, the richest biotite layer is found at 271.8 m and may correspond to the level CQ-274 of Montanari et al. (1985). A few isolated levels with very scarce biotite are found in the stratigraphic interval between these two main clusters, at 253.2 m and 257.5 m, respectively. Finally, an isolated volcaniclastic layer containing sparse but relatively large biotite flakes is found at 282 m. The ~2-meter difference between the location of the dated biotite level CQ-GAR at 274 m in the original Contessa Quarry section and in the new CBR-271.8 is probably due to stratigraphic measuring inaccuracy, and perhaps also to the effect of several unaccounted-for small displacement faults reported by Lowrie et al. (1982) in the middle part of the Contessa Quarry section.

In the 58-m–thick Pieve d'Accinelli section, several thin, volcaniclastic, biotite-rich layers are found throughout the section (Fig. 7).

The studied portion of the Monte Cagnero section covers the middle part of the Oligocene, from meter level 139 up to meter level 223 (Fig. 9). The meter system here has been established with meter level 100 to be stratigraphically equivalent to meter level 0 of the GSSP for the Eocene/Oligocene boundary at Massignano (Premoli Silva and Jenkins, 1993). From 209 m up to the top of the section, the sedimentary succession shows an increase in marly layers, which prevail on the marly limestones. Several biotite-rich levels occur at the base of the Monte Cagnero section from 143 m to 151 m and at 173.5 m and 208 m (Fig. 9).

TABLE 1. STRATIGRAPHIC POSITION (METERS) OF THE CALCAREOUS PLANKTON (PLANKTONIC FORAMINIFERA AND CALCAREOUS NANNOFOSSILS) AND DINOFLAGELLATE CYST EVENTS IN THE STUDIED SECTIONS

Bioevents	CBR	PAC	MCA
Planktonic foraminifera			
LO *Pseudohastigerina naguewichiensis*	241		
FO *Globoquadrina sellii*	244		
LO *Subbotina eocaena*	245		
LO *Pseudohastigerina micra*	247		
FO *Paragloborotalia opima*	250		141.5
LO *Turborotalia ampliapertura*	259		169
FO *Globigerina ciperoensis ciperoensis*	259		164
FO *Zeaglobigerina brazieri*	261		
LO *Subbotina angiporoides*		16	160.5
FO *Tenuitellinata angustiumbilicata*		19	
FO *Globigerina angulisuturalis*	266	20	178
LCO *Chiloguembelina cubensis*	272	27	188
FO *Zeaglobigerina labiacrassata*		36	
FO *Globigerinita juvenilis*		36	
FO *Globigerinella obesa*		43	
LO *Paragloborotalia opima*	288	50	213
FO *Globigerinoides primordius*		50	
FO *Protentella* spp.		51	
FO *Globigerina binaiensis*		54.5	
Calcareous nannofossils			
LO *Sphenolithus akropodus*	247/248		146/147
LO *Reticulofenestra circus*	251/251.5		152/153
LCO *Helicosphaera ethologa*	253/254		156/157
Sphenolithus predistentus/*Sphenolithus distentus* reversal	257/258		165/166
FO *Sphenolithus ciperoensis*	258/259		164/165
LCO *Helicosphaera compacta*	259/260		168/169
LO *Discoaster tanii nodifer*	267.7/268	23/23.5	182/183
FCO *Cyclicargolithus abisectus* > 12 µm	276/277	30/30.5	191/192
LO *Sphenolithus predistentus*	277/278	35.5/36	195/196
LCO *Sphenolithus distentus*	279/280	36.5/37	200/201
Dinoflagellate cysts			
FO *Homotrybilium* sp. cf. *H. oceanicum*			155
FO *Chiropteridium lobospinosum*			175
Chiropteridium spp. pulse		17, 4	183, 202, 211, 222
FO *Distatodinium biffii*	279	35.5	191
Svalbardella abundance interval	276/281	37/43.5	200/208
LO *Wetzeliella gochtii*		43	
FO *Artemisiocysta cladodichotoma*		47	
FO *Membranilarnacia picena*		49	
FO *Caligodinium pychnum*		56	206

Note: CBR—Contessa Barbetti Road; MCA—Monte Cagnero; PAC—Pieve d'Accinelli; FO—first occurrence; LO—last occurrence; FCO—first common occurrence; LCO—last common occurrence.

Biostratigraphy

Planktonic Foraminifera

Planktonic foraminifera are very abundant and well diversified, with preservation ranging from poor to moderate. Reworked specimens from older stratigraphic levels are rare and discontinuous. The assemblages are dominated by catapsydracids, dentoglobigerinids, large globigerinids, globoquadrinids, and globorotaloidids in the coarser fraction, and by tenuitellids, tenuitellinatids, chiloguembelinids, and cassigerinellids in the finer fraction.

Some bioevents recognized in the studied sections are known to have a worldwide chronostratigraphic value (Figs. 5, 7, 9, and Table 1) providing the identification of the planktonic foraminiferal Zones O1 up to top O6.

In particular, according to Berggren and Miller (1988), Nocchi et al. (1988), Berggren et al. (1995), and Berggren and Pearson (2005), the absence of hantkeninids and of the *T. cerroazulensis* group indicates that the lower part of the Contessa Barbetti Road section falls within Zone O1 (Fig. 5).

The absence of *P. naguewichiensis* and the presence of *G. sellii* and *P. opima* allowed us to assign the lower part of the Pieve d'Accinelli section to Zone O3 (Fig. 7).

Finally, in the Monte Cagnero section, the FOs of *P. opima* and *G. ciperoensis ciperoensis* with the LO of *T. ampliapertura* allowed us to assign the lower part of the section to Zone O2 (Fig. 9 and Table 1). In all of the studied sections, the LCO of *C. cubensis* (Figs. 5, 7, 9, and Table 1), which is historically used to approximate the Rupelian/Chattian boundary, is clearly recognizable.

Calcareous Nannofossils

Calcareous nannofossil assemblages are abundant and moderately overgrown in all of the studied sections; species richness varies approximately between 15 and 20. The calcareous nannofossil content is mainly composed by *C. pelagicus, D. bisectus, C. floridanus, C. abisectus, D. deflandrei,* and *S. moriformis.*

Reexamination of the calcareous nannofossil assemblages at the Contessa Barbetti Road section allows the identification of the NP23/NP24 zonal boundary based on the FO of *S. ciperoensis* (Fig. 5). Lowrie et al. (1982) in the Contessa Quarry section recognized the FO of *S. ciperoensis* only above the LO of *S. distentus*. Consequently, they could not define Zone NP24. Moreover, the distinct decrease in abundance (LCO) of the *S. distentus* was used to identify the NP24/NP25 zonal boundary (Fig. 5). Several secondary bioevents have also been recorded in the section, and their abundance patterns and reliability are discussed in Maiorano and Monechi (2006). All the recognized events at Contessa Barbetti Road section are shown in Figure 5 and Table 1.

Quantitative patterns of calcareous nannofossils at Monte Cagnero section are shown in Maiorano and Monechi (2006). We recognized the LCO of *S. distentus,* which identifies the NP24/NP25 zonal boundary, along with a few other supplementary bioevents, as shown in Figure 7 and Table 1.

Previous studies on the Oligocene calcareous nannofossil content of the Monte Cagnero section were performed by Baumann and Roth (1969), Roth (1970), and reinvestigated for the Eocene-Oligocene interval by Madile and Monechi in Parisi et al. (1988). Roth (1970) recognized several important markers from the upper Eocene to the upper Oligocene. The interval between Zone NP23 and Zone NP25 was reinvestigated in this study (Fig. 9 and Table 1; see also Maiorano and Monechi, 2006).

Dinoflagellate Cysts

All samples contain rich assemblages of relatively well preserved palynomorphs. In general, samples are dominated by bisaccate pollen. Dinocysts are the next most abundant palynomorph group. To extract a suite of biostratigraphically relevant dinocyst events, first and last occurrences of taxa in the sections are evaluated (Figs. 5, 7, 9, and Table 1). This evaluation led to the recognition of the following zones and auxiliary bioevents: In the Contessa Barbetti Road section, the FO of *Distatodinium biffii* (Fig. 5 and Table 1) allows the identification of the *Chiropteridium lobosinosum* (Clo)/*Distatodinium biffii* (Dbi) zonal boundary. The *Svalbardella* abundance interval of Van Simaeys et al. (2005) falls in the interval including the Clo-Dbi transition (Fig. 5); in the Pieve d'Accinelli section (Fig. 7), the *C. lobospinosum* (Clo) Zone (from 2 m up to 35.5 m), and the lower part of the *D. biffii* (Dbi) Zone (from 35.5 m up to 58 m). In the lower part of the Dbi Zone, the recognition of the *Svalbardella* abundance interval of Van Simaeys et al. (2005) and the LO of *Wetzeliella gochtii* (Fig. 7 and Table 1) are of importance and allow further subdivision of this zone (cf. Wilpshaar et al., 1996). Of note, two pulses in abundance of *Chiropteridium* spp. (>50% of total dinocyst assemblage) are recorded (Fig. 7 and Table 1): (1) in the Monte Cagnero section, the middle-upper part of the *Hystrichokolpoma pusilla* (Hpu) Zone (from 139 m to ~175 m), the entire *C. lobospinosum* (Clo) Zone (from ~175 m to ~191 m), and (2) the *D. biffii* (Dbi) Zone (from ~191 m to ~223 m) (Fig. 9). Following Brinkhuis et al. (1992), the identification of the "youngest *Chiropteridium* spp. pulse" at ~222 should permit the identification within the Dbi Zone of the lower *Hystrichosphaeropsis* sp.—cf. *H. obscura* (Hob) Subzone (from ~191 m to ~222 m) and the upper *Chiropteridium* (Chi) abundance Subzone (from ~222 m to ~223 m) (Fig. 9). Remarkably, four pulses in abundance of *Chiropteridium* spp. are recorded, at ~183 m, ~202 m, ~211 m, and ~222 m (Fig. 9 and Table 1).

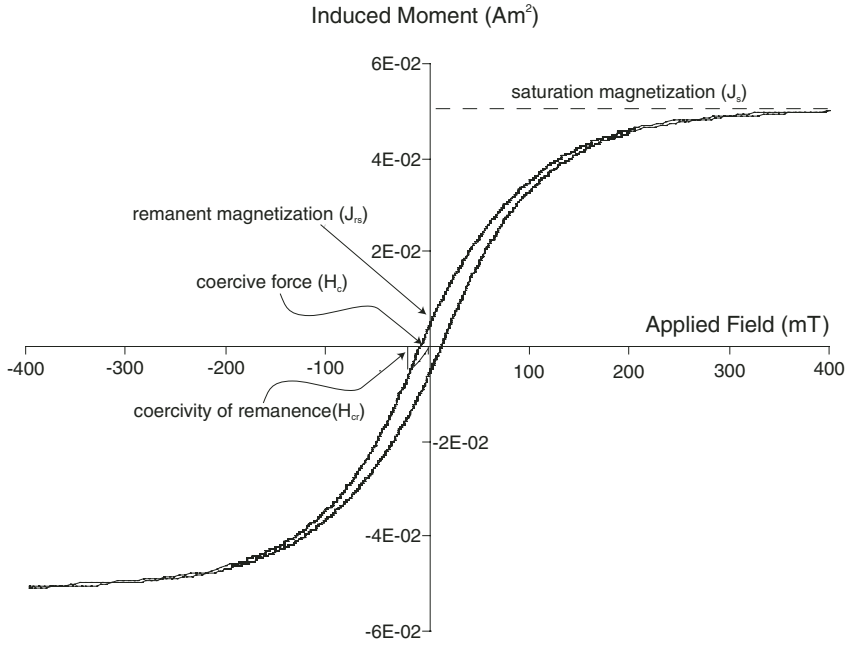

Figure 10. Hysteresis loop for sample Pieve d'Accinelli (PAC) 12.05, corrected for high field slope. The values for determining the size of a magnetite grain are J_s, J_{rs}, H_c, and H_{cr}. H_{cr} represents the reverse field that, when applied and removed, cancels the J_{rs} value to make the magnetization of the sample zero.

Magnetostratigraphy

Previous studies of the magnetic properties of the Scaglia Cinerea (Lowrie et al., 1982) have concluded that magnetite is the primary magnetic mineral of these rocks. Our studies generally confirm this result, with very consistent results from the three sections. The hysteresis properties (Fig. 10) show high susceptibility, low coercivity, and saturation at low applied fields. This relatively low coercivity is a strong indicator of magnetite particles, which have maximum coercivities around 0.3 T, as opposed to hematite, which has a range of coercivity between 0.5 and 5.0 T (Lowrie, 1997). Demagnetization behaviors are similar for the Contessa Barbetti Road and Pieve d'Accinelli sections (Fig. 11), with a weak overprint, a generally univectorial demagnetization path between 20 and 50 mT, and less

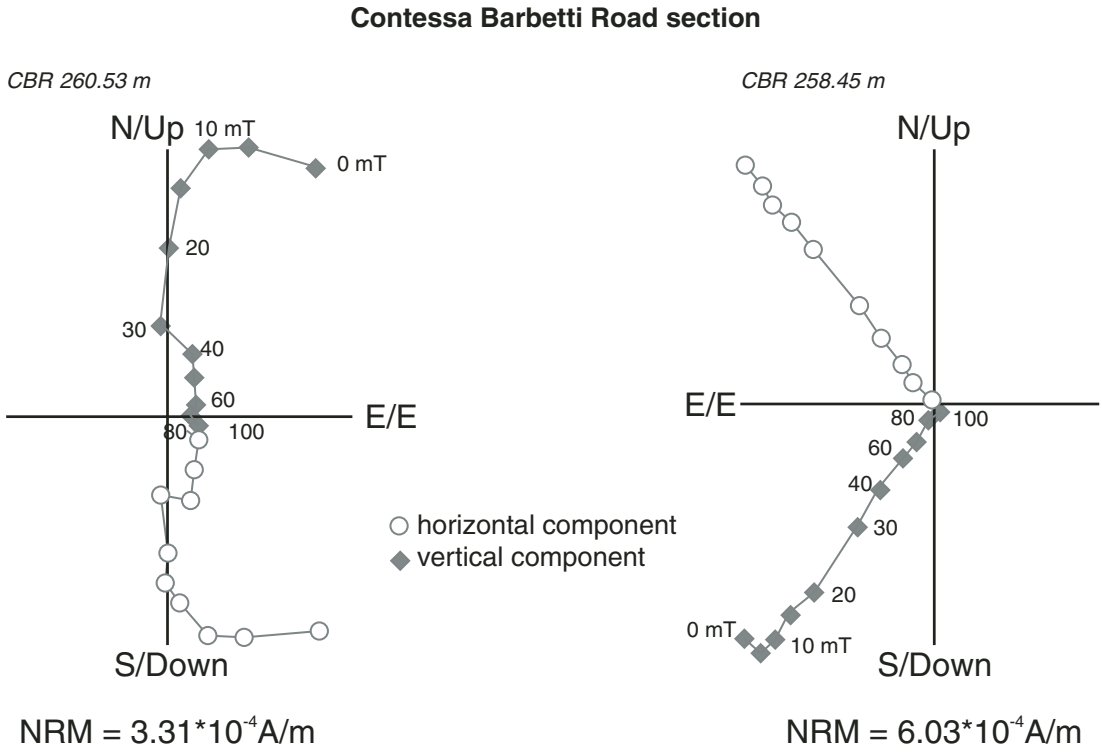

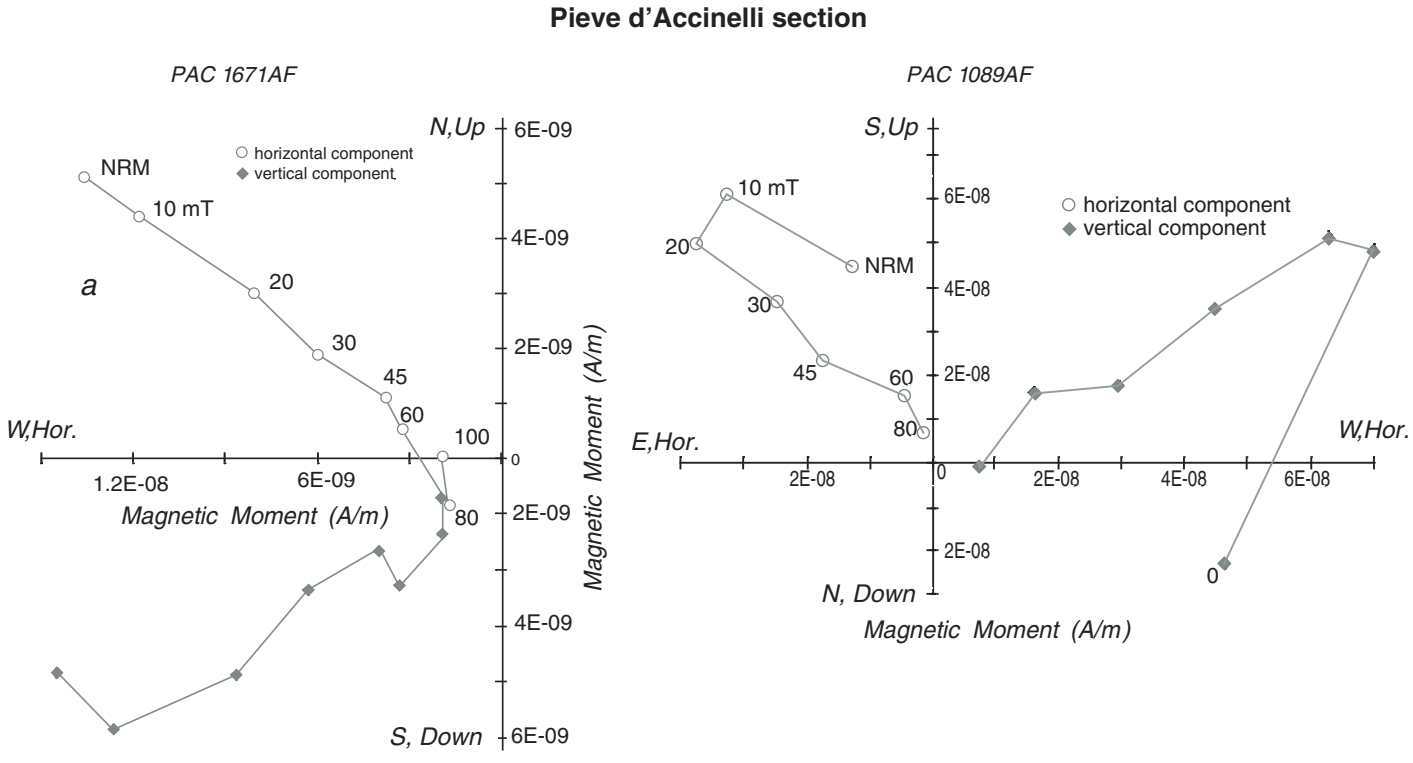

Figure 11. Zijderveld orthogonal projection diagrams of alternating field (AF) demagnetization behavior of representative samples from the Contessa Barbetti Road (CBR) and Pieve d'Accinelli (PAC) sections. NRM—natural remanent magnetization.

than 5% of the initial NRM intensity remaining at 100 mT. Most ChRM directions are thus easily defined by principal component analysis. In some samples, however, the secondary component is more prominent and the lack of linear demagnetization path pointing to the origin in orthogonal projections led us to use linear fits not anchored to the origin (Fig. 11) or, in the worst cases, only the direction at the higher significant demagnetization step. In a few samples, the persistence of some NRM even under high alternating fields (Fig. 11) indicates the presence of a minor amount of higher coercivity mineral (Fig. 10), probably hematite, which is an abundant magnetic mineral in other Scaglia limestones (Lowrie, 1997). The S-ratio in Contessa Barbetti Road samples that we analyzed confirms previous observations by Lowrie et al. (1982) that magnetite is the main magnetic mineral in the Scaglia Cinerea, with values ranging, in most of the cases, between –1.0 and –0.97.

When plotting all ChRM directions on equal-area spherical projections (Fig. 12), antipodal and well-clustered normal and reverse directions are observed with very few intermediate directions. Mean declination and inclination values are typical of expected counterclockwise-rotated and shallow paleomagnetic directions for the Oligocene of this sector of the northern Apennines (Lowrie et al., 1982). This is a further confirmation of the primary nature of the measured ChRM.

The magnetostratigraphic interpretation of the Contessa Barbetti Road section shown in Figure 5 confirms the polarity sequence originally defined by Lowrie et al. (1982). Although

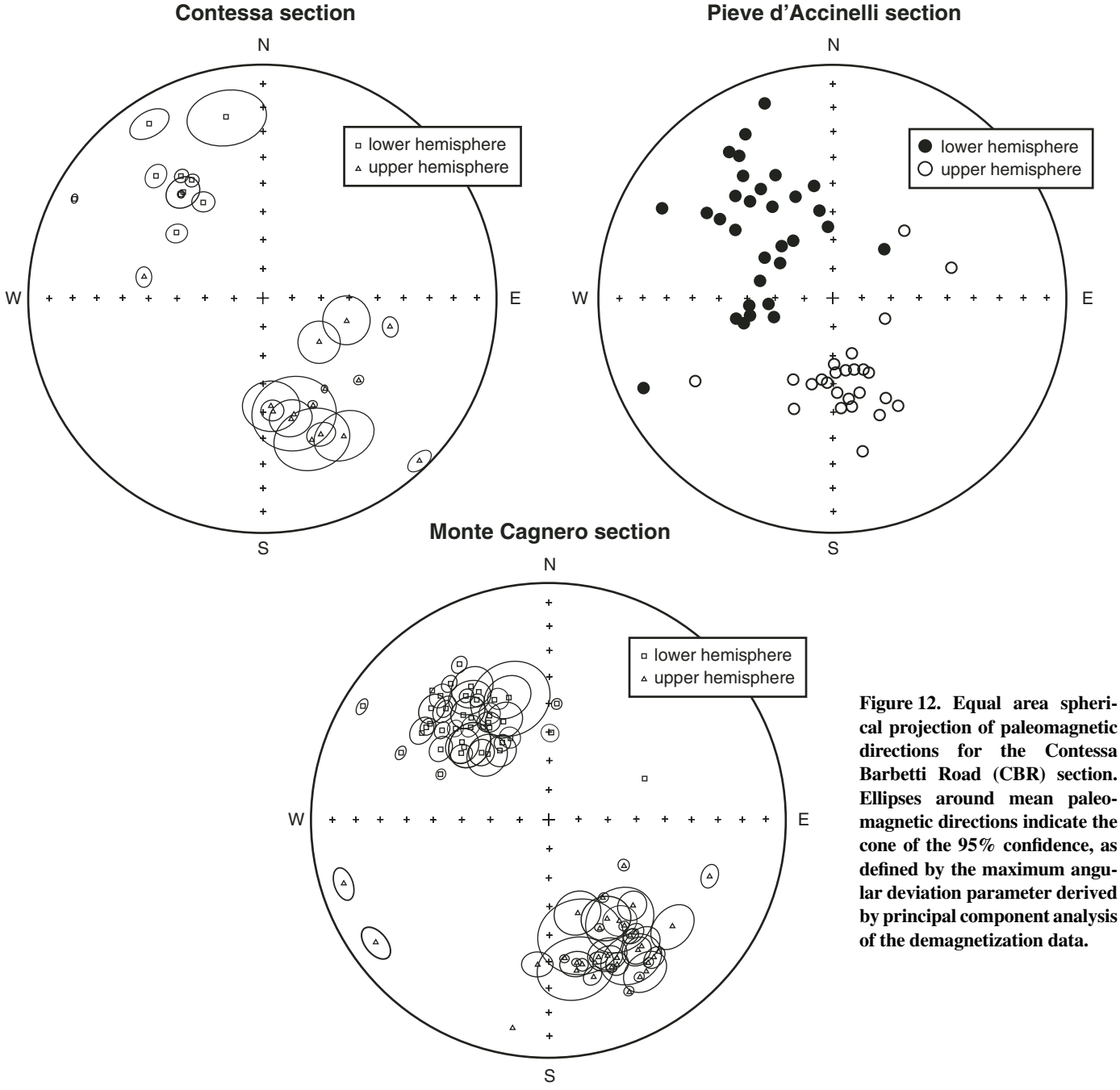

Figure 12. Equal area spherical projection of paleomagnetic directions for the Contessa Barbetti Road (CBR) section. Ellipses around mean paleomagnetic directions indicate the cone of the 95% confidence, as defined by the maximum angular deviation parameter derived by principal component analysis of the demagnetization data.

some polarity zones are identified by just one or two samples, the close agreement with the work of Lowrie et al. (1982) lends confidence to the Contessa Barbetti Road polarity sequence.

The Pieve d'Accinelli section records an apparently continuous and complete record of magnetic polarity reversals from the uppermost Chron 11n to the lower Chron 8r (Fig. 7). We interpret the normal polarity interval between 32.5 m and 43 m as C9n based on the fact that it contains both the boundaries between planktonic foraminiferal Subzones P21a and P21b (O4/O5 of Berggren and Pearson 2005), and calcareous nannofossil Zones NP24 and NP25. In fact, these biostratigraphic boundaries are found in the same magnetostratigraphic zone in the classic Contessa section, reanalyzed in this work (see above), and in the Monte Cagnero section discussed below.

The relatively strong weathering of the natural slope exposure of the Monte Cagnero section, when compared to the recently quarried Contessa sections, have resulted in more development of hematite and more common secondary components. In fact, the ChRM directions identified in the Monte Cagnero section include some intermediate directions (Fig. 12), suggesting some post-depositional remagnetization, which may slightly blur the magnetic reversal positions.

The magnetostratigraphic interpretation of the Monte Cagnero section is relatively straightforward, and allows the recognition of all the polarity reversals from the top of Chron 12r to the base of Chron 8r (Fig. 9). However, some uncertainty remains in interpreting short polarity subzones within Chron 12n, Chron 11n, and Chron 9n, which are represented by few samples with intermediate polarity.

Isotope Stratigraphy

Oxygen and Carbon Isotopes

The high-resolution $\delta^{13}C$ data from the Pieve d'Accinelli section (Fig. 7) range from 0.8‰ to 1.3‰, which is typical of normal marine surface waters, and there are no signs of significant alteration of the signal. In contrast, the $\delta^{18}O$ values average ~−1.5‰, much lighter than expected, and almost certainly reflect the influence of meteoric waters. The carbon isotope data show clear cycles that match the astronomical cycles (Fig. 7), especially the ~100 k.y. eccentricity for this time period. The general character of these cycles, in which peaks in $\delta^{13}C$ are associated with peaks in eccentricity, tilt, and precession (ETP), and peaks in carbonate content, are similar to the glacio-eustatic productivity cycles identified by Wade and Pälike (2004) from the Pacific. The dominance of the 100 k.y. cycle is partly a result of the sampling interval of 15 cm, which translates to ~15 k.y., making detection of the ~20 k.y. precessional cycles unlikely. Nevertheless, the strength of the correlation between the Pieve d'Accinelli $\delta^{13}C$ signal and the astronomical ETP signal indicates a high-fidelity recording of astronomically driven climate cycles, making this section a good candidate for more detailed astrochronologic calibration of the Oligocene. The Pieve d'Accinelli $\delta^{13}C$ record also matches the Ocean Drilling Program (ODP) Site 1218 isotopic record from the equatorial Pacific (Wade and Pälike, 2004), especially during the time period near the upper part of magnetozone 9n2n. The Pieve d'Accinelli oxygen isotope record is not as clearly associated with the astronomical variations, but it does show a notable similarity to the ODP Site 1218 record in the vicinity of the glacial event Oi-2a (Fig. 7), which essentially spans the Rupelian/Chattian boundary.

Carbon and oxygen stable isotope data (Fig. 9) from the Monte Cagnero section provide yet another means for correlation with other sections around the globe, although the coarser sampling interval in this study precludes any correlation with astronomical cycles as was possible for part of the Pieve d'Accinelli section. The Monte Cagnero $\delta^{13}C$ signal shows an average value of about ~1.7‰ from the base of the section up to the middle of magnetic chronozone C12n. Then, a negative excursion shifts the mean values to averages of ~1.0‰ from the top of the C11n.1n to the top of the studied section. Superimposed on this long-term trend, short fluctuations shift the isotope record in the range of ±0.75‰. The long-term negative $\delta^{13}C$ excursion is consistent with the global record during this time period (Zachos et al., 2001) and most likely represents a decrease in the burial and preservation of isotopically light organic carbon due to greater oxygenation of the deep ocean following the establishment of Antarctic ice sheets (Zachos et al., 2001). The $\delta^{18}O$ record shows a slight negative excursion of ~0.2‰ from the base of the section, where averages of ~−1.6‰ were measured, up to the top of the C8r magnetic chron; shorter-term ±0.7‰ oscillations are superimposed on this negative excursion. Although the $\delta^{18}O$ values are all more negative than the oceanic record during this time period (e.g., Wade and Pälike, 2004), the lack of covariance between $\delta^{18}O$ and $\delta^{13}C$ suggests a limited influence of meteoric or burial diagenesis on the isotope signatures. Overall, the $\delta^{18}O$ pattern observed at the Monte Cagnero section matches fairly well the open ocean record (Fig. 9), both in shape and magnitude of oscillations; this enables us to identify several of the Oligocene glacial events of Miller et al. (1991), and demonstrates that the stable isotope record preserved in the Monte Cagnero section reflects paleoceanographic and paleoclimatic events of global significance.

Sr Isotopes

The most striking feature of the $^{87}Sr/^{86}Sr$ profile from the Pieve d'Accinelli section is a shift at ~30 m from mean values ~0.70805–0.70813 at ~37 m, and a second shift at 53.5 m from 0.70813 to 0.70817 up to the end of the section (Fig. 7 and Table 3).

The reliability of Sr isotopic values from bulk carbonate samples from the Eocene to uppermost Miocene pelagic limestone and marls of the Umbria-Marche succession has been assessed in two principal ways—by comparing $^{87}Sr/^{86}Sr$ values from different mineral phases within the same layer, and by comparing identical layers from widely spaced locations. Apatite is expected to be less susceptible to diagenetic change than calcite, but Montanari et al. (1991) found no variation in $^{87}Sr/^{86}Sr$ values from bulk carbonate and phosphatic fish teeth from the same limestone layer, suggesting no diagenetic bias in bulk carbonate samples.

The $^{87}Sr/^{86}Sr$ values of the lowermost and uppermost samples from the Pieve d'Accinelli section are consistent with the values obtained from bulk-rock samples from stratigraphically equivalent levels in the composite Contessa Quarry–Contessa Testimone (CQ-CT) section obtained by Montanari et al. (1991), although the two sections are more than 15 km apart. Moreover, the values obtained from the three samples of the Monte Cagnero section are very consistent with stratigraphically equivalent samples from the Pieve d'Accinelli section (Fig. 7), further increasing our confidence that these values do, in fact, represent original seawater composition.

The interpretation of the $^{87}Sr/^{86}Sr$ curve from the Pieve d'Accinelli section requires a comparison with the whole Sr record of the Umbria-Marche sequence, and with the record from coeval oceanic sediments (Reilly et al., 2002; correlated to our sections on the basis of magnetostratigraphy), as shown in Figure 13. In addition, such an interpretation must also consider variations of sea level, and the paleogeographic evolution of the Mediterranean region. The basic assumption is that the seawater $^{87}Sr/^{86}Sr$ ratio varies through time in response to relative changes in three main influxes: (1) weathering of oceanic basalts and seafloor hydrothermal activity ($^{87}Sr/^{86}Sr$ around 0.703); (2) weathering of continental crystalline rocks ($^{87}Sr/^{86}Sr$ ~0.714); and (3) recycled Sr from exposed and eroded carbonate shelves ($^{87}Sr/^{86}Sr$ ratios in Cretaceous to early Eocene

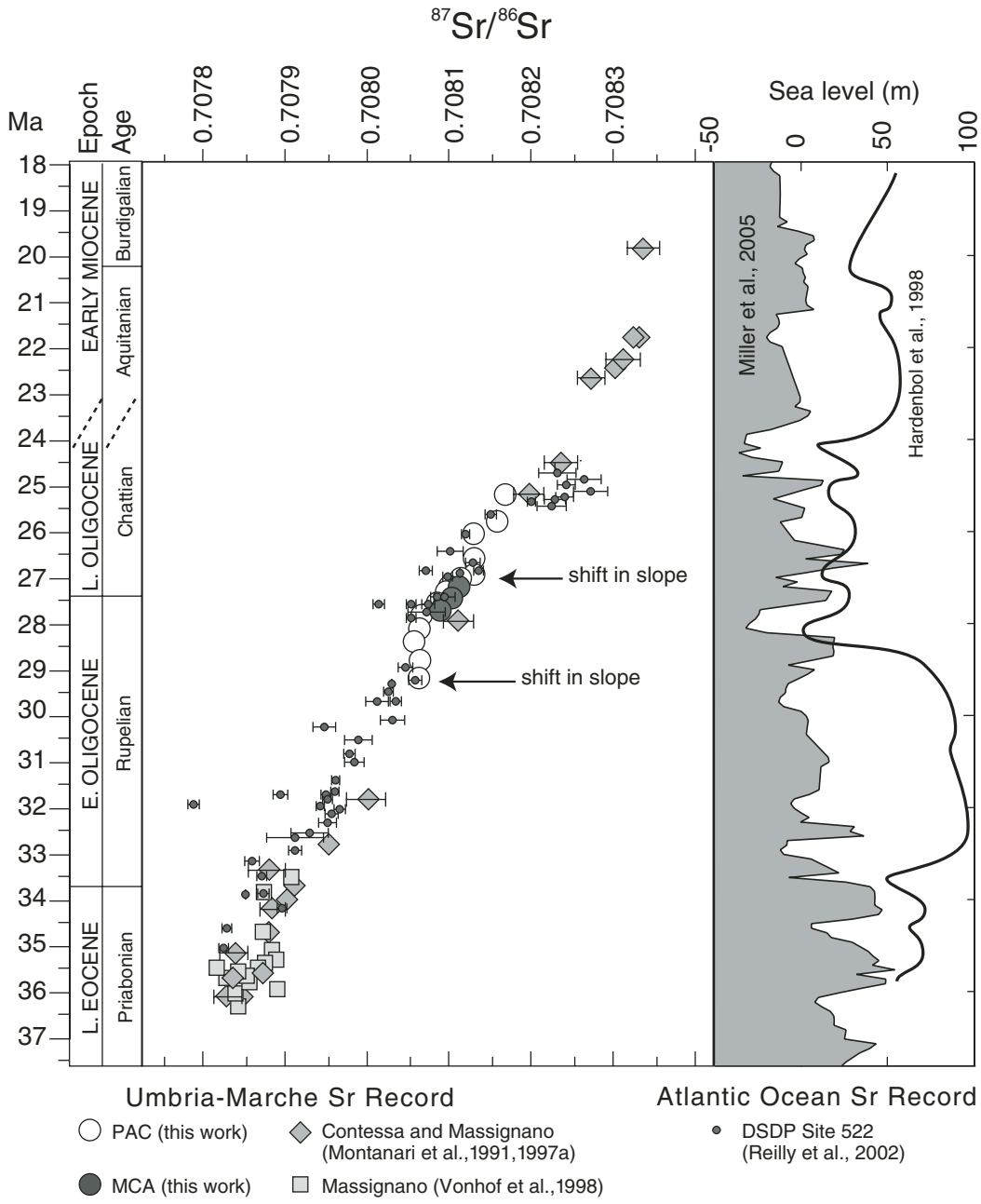

Figure 13. The strontium isotope record of the Umbria-Marche succession compared with the oceanic Sr record and Eocene-Oligocene eustatic curves. The oceanic Sr record was correlated to the Umbria-Marche data using the magnetic reversal stratigraphy, and then to geochronologic ages using the dates presented here.

carbonate rocks range between 0.707 and 0.708, and are significantly lower than ratios around 0.708–0.709 for late Eocene to Pliocene marine carbonate rocks). The rate of $^{87}Sr/^{86}Sr$ change in the South Atlantic record (Deep Sea Drilling Project [DSDP] 522) is linear at ~5 × 10^{-5}/m.y. throughout the late Eocene and late Oligocene (Fig. 13).

In the upper Chattian, within foraminiferal Zone O6, the Sr isotopic record shifts to a lower rate of change of 2 × 10^{-5}/m.y. Such a flexure was interpreted by Capo et al. (1991) as a consequence of a relative low sea-level stand, which, after the large (but controversial) sea-level drop recorded at the Rupelian/Chattian boundary by Schlanger and Premoli Silva (1986) in the mid-Pacific, persisted for several million years until the mid-Burdigalian. Capo et al. (1991) proposed that such a conspicuous eustatic event would have caused erosion of exposed carbonate shelves with consequent dissolution and recycling of Sr components with lower isotopic ratios (i.e., Cretaceous and Lower Tertiary marine carbonates), which would have lowered the rate of increase of the $^{87}Sr/^{86}Sr$ in seawater.

The Umbria-Marche Sr isotopic record is broadly consistent with the South Atlantic record throughout the time period considered here, but the higher resolution from the Monte Cagnero section reveals two small steps in the interval near the Rupelian/Chattian boundary (Fig. 13). Close to the O3/O4 zonal boundary, the Pieve d'Accinelli Sr curve shifts to a lower slope; after a short stretch of lower slope, just prior to the O4/O5 zonal boundary (i.e., the Rupelian/Chattian boundary), the Pieve d'Accinelli Sr curve shifts back to a higher slope with a linear slope similar to the oceanic curve (Fig. 7); a similar, though slightly smaller step, begins just after this first step, and is near the middle of zone O6. These steps appear to correlate with eustatic drops that show up in the Hardenbol et al. (1998) curve,

TABLE 2. SUMMARY INCREMENTAL-HEATING AGES OF BIOTITES AND PLAGIOCLASES FROM CONTESSA QUARRIES SECTIONS: PLATEAU AND INTEGRATED AGE CALCULATIONS

Sample	Mineral	Result type	Plateau age	n	MSWD	% Gas	Integrated age
CBR98-271.8	Bi	Plateau	29.02 ± 0.10	5 (D-H)	0.79	56	28.60 ± 0.09
CBR98-271.8	Bi	No plateaus					28.64 ± 0.09
CBR98-271.8 P40-80	Plag	No plateaus					32.00 ± 10.00
CBR98-271.8 P80-100	Plag	Plateau	43.30 ± 1.20	6 (A-F)	0.70	64	49.00 ± 10.00
CQ-GAR	Bi	Plateau	29.17 ± 0.10	10 (F-O)	1.25	72	28.71 ± 0.09
CQ-GAR	Bi	Plateau	29.07 ± 0.12	8 (H-O)	1.78	51	28.60 ± 0.09

Note: All ages are in units of Ma with uncertainties given at 1σ. Bi—Biotite; Plag.—Plagioclase; MSWD—Mean Square of Weighted Deviates, a parameter that assesses magnitude of the observed scatter of the ages of the steps included in the plateau, compared to their analytical scatter; n—Number of steps included in the plateau.

and to a lesser extent, the Miller et al. (2005) curve (Fig. 13), and the nature of these steps is consistent with the addition of older recycled carbonates from emergent shelves. However, the fact that these two steps in the Sr curve are nearly equal in magnitude, along with the observation that not all eustatic drops can be tied to a step in the Sr curve, makes a simple cause-and-effect relationship with eustatic drops a bit tenuous. Nevertheless, these steps are compatible with the existing data from the Atlantic, and the Pieve d'Accinelli Sr data that reveal these steps appear to be reliable.

Geochronology

Biotite concentrates from samples CQ-GAR and CBR-271.8 were analyzed four and two times, respectively, by $^{40}Ar/^{39}Ar$ incremental-heating technique (Table 2). One $^{40}Ar/^{39}Ar$ analysis was also carried out on a plagioclase separate from sample CBR-271.8. The spectra of these analyses are shown in Figure 14. In data analysis, we are accepting the commonly used criteria for the detection of a "plateau" expressed by Fleck et al. (1977): a plateau consists of a minimum of three contiguous steps comprising at least 50% of the total ^{39}Ar released, in which all step ages are mutually indistinguishable at the 95% confidence level. All plateau and integrated ages are reported at the 2σ level, and incorporate the error in *J*, the neutron fluence parameter. All the biotite spectra are characteristic of mild recoil (Fig. 14). These spectra begin with low, geologically unreasonable, initial apparent ages, quickly stair-stepping upward in an approach to the "true" age.

Apparent ages may reach a broad maximum, then decrease slightly during the latter half or third of the experiment. Spectral characteristics of this type may originate in biotites as the result of recoil emplacement of ^{39}Ar generated during irradiation from the biotite lattice into comparatively poorly retentive interlayer chlorite and vermiculite sites.

This component of the ^{39}Ar is then lost preferentially during the early phases of the incremental-heating experiment, resulting initially in artificially low apparent ages (Lo and Onstott, 1989; Lo et al., 2000; Min et al., 2001). Although four of six biotite incremental heating experiments attained plateaus, all encompassed less than ~70% of the ^{39}Ar release.

In almost all cases, these plateaus rest on spectra that are rising, falling, or humped. In most of these cases, the integrated ages are within error of the plateau ages, suggesting that these results may closely approach the true geologic age. Nevertheless, it is imprudent to use these results for time scale calibration in light of the internal evidence for disturbance of the argon isotopic systematics.

Biotite concentrates from four samples collected in the Monte Cagnero section at meter levels 145.5 (sample MCA-3), 207.7 (sample MCA98-6), and 208.3 (sample MCA-7) were analyzed two to five times for an overall total of 13 $^{40}Ar/^{39}Ar$ experiments (Table 4). For this collection of samples, we used the same sample preparation, analytical methods, and techniques as the ones we already described for the Contessa Quarry and Contessa Barbetti Road sections. The observed biotite spectra exhibit a wide range of behavior. The majority are characteristic of mild recoil (Figs. 15C, 15D, 15E, and possibly 15G), as seen in most of biotite samples from the Contessa sections. The second most common spectral type (Figs. 15A, 15B, and 15I) decreases markedly in apparent age throughout the first half of the experiment before forming a plateau. Several spectra decrease subtly throughout the course of stepwise heating (three spectra attributable to one sample; Figs. 15J, 15L, and 15M), but are probably just less severe variants of the former.

This type of discordance may reflect alteration of the biotite in such a manner as to remove K preferentially to Ar, but which does not generate significant interlayer chlorite or mask the recoil effect. Two biotite spectra exhibit marked discordance after having reached a "plateau" of reasonable geologic age (Figs. 15F and 15I). In the case of sample MCA98-6 (Fig. 15I), a plagioclase separate was also analyzed, and this material exhibited extreme discordance, with apparent ages reaching ca. 400 Ma and integrated ages about ten times the geologic age (Figs. 15N and 15O). Thus a possible explanation for spectrum 15I is that a minor amount of fine plagioclase is present in the biotite separate, either as inclusions or discrete grains. Spectrum 15F may also be explained in this fashion, although plagioclase from this sample was not analyzed. Only two spectra form plateaus across more than 90% of the ^{39}Ar release. Figures 15E and 15H both exhibit behaviors suggestive of minor recoil. Figure 15E has large uncertainties in apparent age in the individual steps due to small aliquot size, and this error envelope masks a progressive stairstep rising pattern that is nevertheless within a statistically defined plateau. The uncertainty in the plateau age is ±0.4 Ma (1.4%), little better than a conventional K-Ar age. On the other hand, Figure 15H yields a much more precise result at 27.15 ± 0.18 Ma for sample MCA98-6. The integrated age is virtually the same at 27.1 ± 0.2 Ma. Although nine of 13 biotite incremental-heating experiments yielded plateaus, other than the two examples cited above, all encompass less than ~70% of the ^{39}Ar release.

As seen in the experiments from the Contessa section samples, in almost all cases these plateaus rest on spectra that are rising, falling, or humped. In many of these cases, the integrated ages are within the error of the plateau ages, suggesting that these results may closely approach the true geologic age. With the exception of biotite samples MCA/84-3, MCA98-6,

TABLE 3. RESULTS FROM STRONTIUM ISOTOPE ANALYSES FROM THE PIEVE D'ACCINELLI (PAC) AND MONTE CAGNERO (MCA) SECTIONS

Sample	Meter	$^{87}Sr/^{86}Sr$	Error × 10^{-5}
PAC1	13.7	0.7080577	0.8
PAC2	17.3	0.7080597	1.0
PAC3	20.8	0.7080509	0.8
PAC4	24.5	0.7080582	0.8
PAC5	28.0	0.7080582	0.8
PAC6	32.0	0.7080791	0.8
PAC7	36.1	0.7080970	1.0
PAC8	9.0	0.7080979	1.0
PAC9	42.0	0.7081172	1.0
PAC10	45.5	0.7081334	1.0
PAC11	49.5	0.7081294	1.0
PAC12	53.5	0.7081306	0.8
PAC13	57.5	0.7081571	1.0
PAC14	58.5	0.7081679	0.8
MCA15	194	0.7080845	1.0
MCA16	198	0.7080982	0.8
MCA17	202	0.7081161	1.0

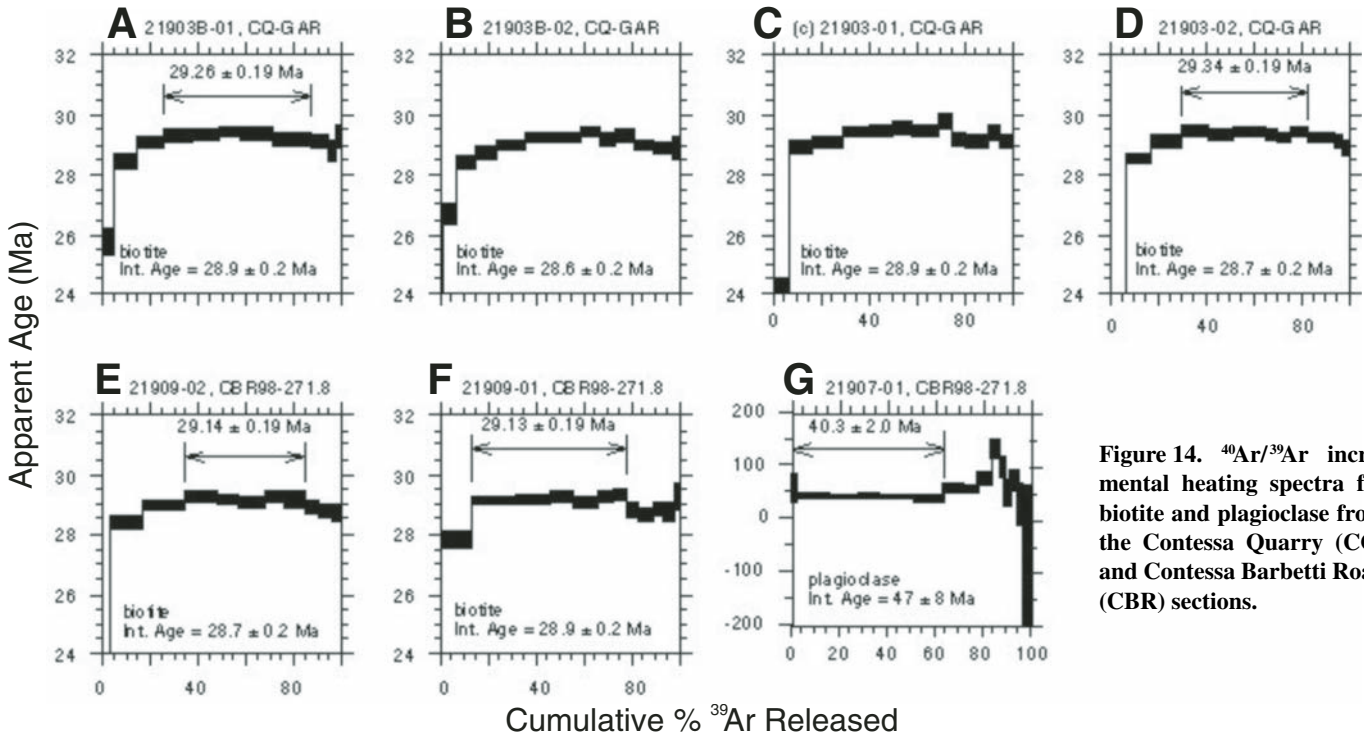

Figure 14. $^{40}Ar/^{39}Ar$ incremental heating spectra for biotite and plagioclase from the Contessa Quarry (CQ) and Contessa Barbetti Road (CBR) sections.

TABLE 4. SUMMARY INCREMENTAL-HEATING AGES OF BIOTITES FROM THE MONTE CAGNERO (MCA) SECTION: PLATEAU AND INTEGRATED AGE CALCULATIONS

Sample	Mineral	Result type	Plateau age	n	MSWD	% Gas	Integrated age
MCA/84-3 KA4853	Bi	Plateau	31.43 ± 0.11	7 (H-N)	1.29	70	31.57 ± 0.10
MCA/84-3 KA4853	Bi	Plateau	31.33 ± 0.10	8 (I-P)	0.75	72	31.52 ± 0.10
MCA/84-5 KA 4729	Bi	Plateau	28.70 ± 0.20	14 (C-P)	0.67	97	28.60 ± 0.20
MCA/84-5 KA#4729 Bi	Bi	No plateaus					29.12 ± 0.12
MCA/84-5 KA#4729 Bi	Bi	Plateau	29.09 ± 0.13	9 (D-L)	1.35	78	28.80 ± 0.11
MCA98-6	Bi	Plateau	27.07 ± 0.09	11 (E-O)	0.78	91	27.02 ± 0.09
MCA98-6	Bi	No plateaus					27.87 ± 0.09
MCA98-7	Bi	Plateau	26.71 ± 0.10	11 (D-N)	0.84	70	26.65 ± 0.09
MCA98-7	Bi	Plateau	26.62 ± 0.10	14 (C-P)	1.37	100	26.63 ± 0.09
MCA98-7 Bi	Bi	Plateau	26.69 ± 0.11	13 (B-N)	1.22	78	26.67 ± 0.09
MCA98-7 Bi	Bi	Plateau	26.61 ± 0.10	5 (L-P)	0.82	61	27.14 ± 0.09

Note: All ages are in units of Ma with uncertainties given at 1σ. Bi—Biotite; MSWD—Mean Square of Weighted Deviates, a parameter that assesses magnitude of the observed scatter of the ages of the steps included in the plateau, compared to their analytical scatter; n—Number of steps included in the plateau.

and MCA98-7, it is imprudent to use these results for time scale calibration in light of the internal evidence for disturbance of the argon isotopic systematics.

SUMMARY AND CONCLUSIONS

Integrated stratigraphic analyses of three apparently continuous and complete pelagic sections spanning the Oligocene epoch in the Umbria-Marche Apennines of Italy, the Contessa Barbetti Road section near Gubbio, the Pieve d'Accinelli section near Piobbico, and the Monte Cagnero section near Urbania, provide a precise calibration of the Rupelian/Chattian stage boundary as it is defined in current chronostratigraphic time scales, on the basis of biostratigraphic, magnetostratigraphic, and chemostratigraphic criteria (Fig. 16). Moreover, new $^{40}Ar/^{39}Ar$ dating of volcaniclastic, biotite-rich layers contained in these pelagic sediments, some of which were dated by the traditional K/Ar method, and the Rb/Sr method in previous works, allows us to reassess the accuracy of existing geochronologic time scales.

In agreement with Berggren and Pearson (2005), the Rupelian/Chattian stage boundary is here placed at the LCO of *Chiloguembelina cubensis* (Figs. 1 and 16). This event marks the boundary between planktonic foraminiferal Zones O4 and O5 of Berggren and Pearson (2005) corresponding to the boundary between Subzones P21a and P21b of Berggren and Miller (1988) and Berggren et al. (1995), and falls within the middle of nannofossil Zone NP24 of Martini (1971) (Fig. 1). Wade et al. (2007) highlight that the synchronous LCO of *C. cubensis* is documented from a number of ODP sites and correlates either directly or indirectly with Chron 10n (e.g., Site 516, Pujol, 1983; Site 558, Miller et al., 1985; Sites 529 and 77B, Hess et al., 1989; and ODP Site 1218). At DSDP Site 522, sporadic occurrences of *C. cubensis* within the *P. opima* Zone are considered by Poore et al. (1982) and Poore (1984) to be reworked, although Leckie et al. (1993) have reported rare occurrences of *C. cubensis* throughout the upper Oligocene.

In the Umbria-Marche basin, the magnetic polarity across the Rupelian/Chattian boundary was defined in the Pieve d'Accinelli and Monte Cagnero sections. In both cases, the O4/O5 zonal boundary falls in the upper half of Chron 10n (Fig. 1), also in agreement with Berggren et al.

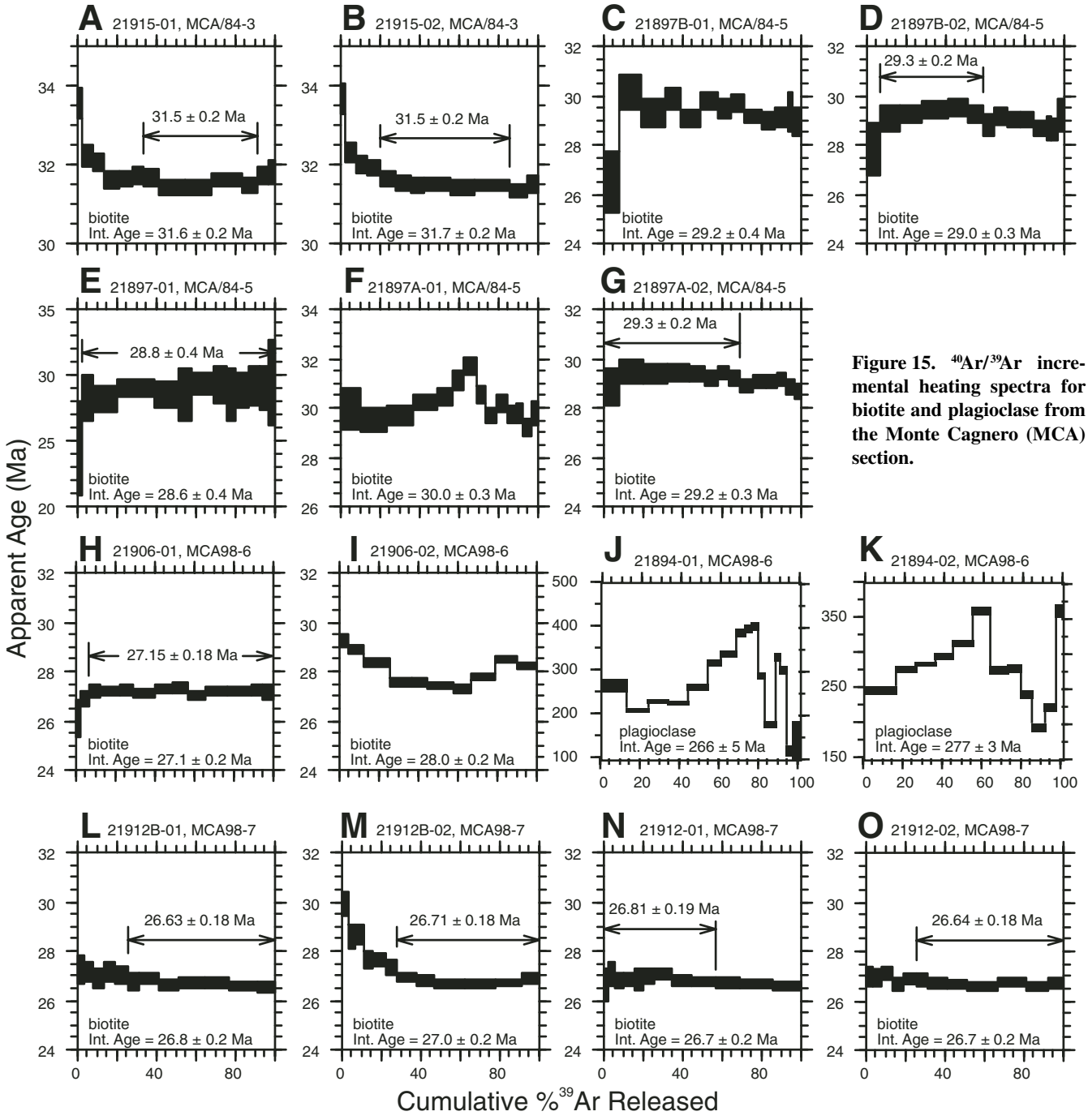

Figure 15. $^{40}Ar/^{39}Ar$ incremental heating spectra for biotite and plagioclase from the Monte Cagnero (MCA) section.

(1995), Luterbacher et al. (2004), and Berggren and Pearson (2005). Our results fit well within this chrono-magnetostratigraphic scenario and, contrary to Van Simaeys et al. (2004), strongly support that the LCO of *C. cubensis* is a robust bioevent for the O4/O5 (P21a/P21b) zonal boundary and correlates to Chron 10n. This correlation is also consistent with many deep-sea records (e.g., Wade et al., 2007).

In all the studied sections, the LCO of *C. cubensis* clearly predates the LCO of the calcareous nannofossil *S. distentus* used here to recognize the NP24/NP25 zonal boundary of Martini (1971) (Fig. 19). In terms of dinoflagellate cyst events, the *Svalbardella* abundance interval of Van Simaeys et al. (2005) falls within Chron 9n (Fig. 16).

The $\delta^{13}C$ record reflects long-term changes that correlate well with those seen throughout the globe, especially a general decline during most of the upper Rupelian, followed by a general, but slight, increase during the Chattian. In addition, there are shorter-term oscillations that parallel the changes in carbonate content—these oscillations likely reflect productivity cycles related to climate changes related to Milankovitch cycles. The relationship observed at the Pieve d'Accinelli section links high ETP values to high productivity (high $\delta^{13}C$) and high carbonate content, similar to the relationship inferred from ODP Site 1218 in the Pacific (Wade and Pälike, 2004). Stable isotope results from both Pieve d'Accinelli and Monte Cagnero indicate

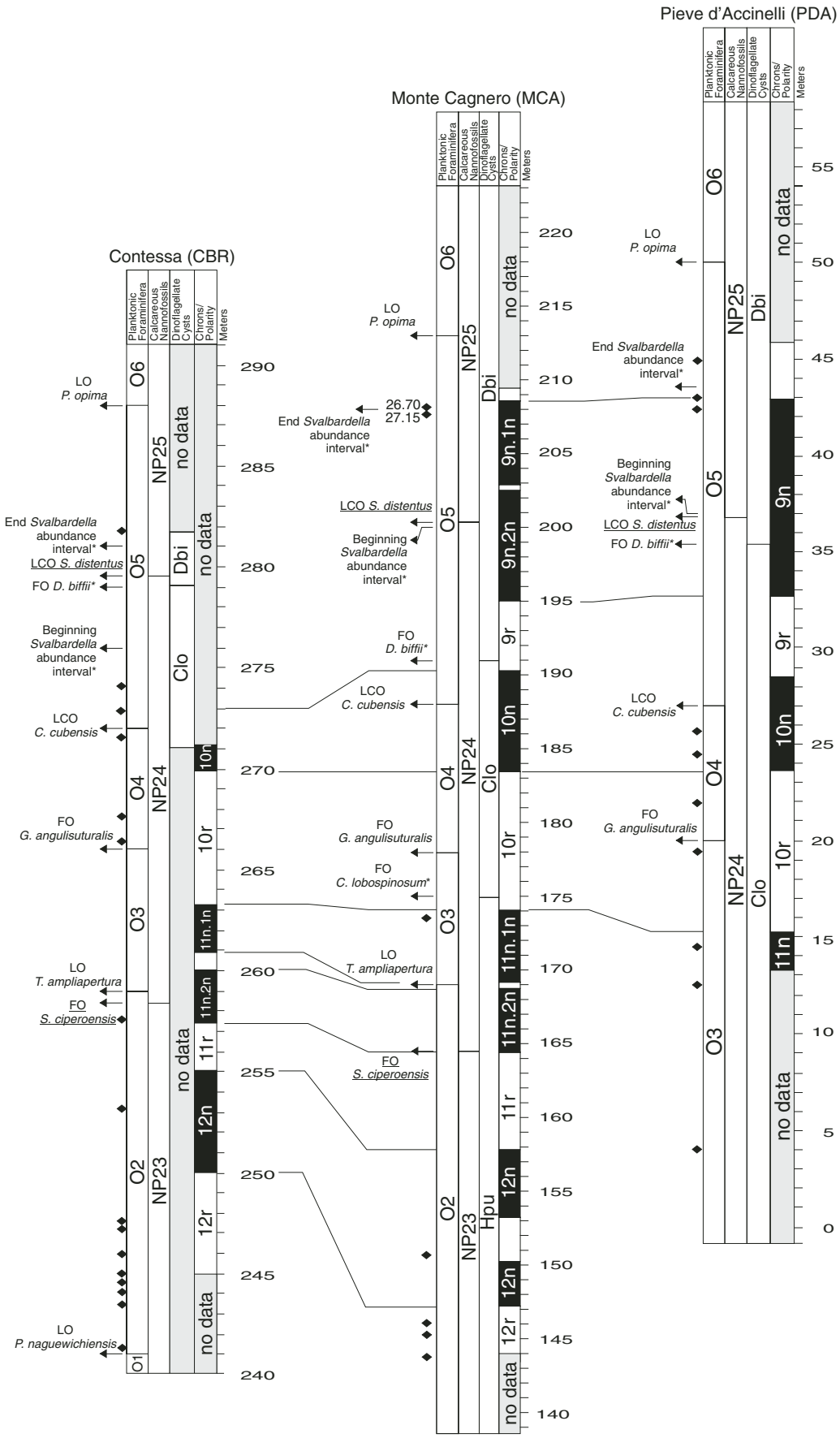

Figure 16. Comparison among the three studied sections in the Umbria-Marche Apennines of Italy. See also Figures 5, 7, and 9.

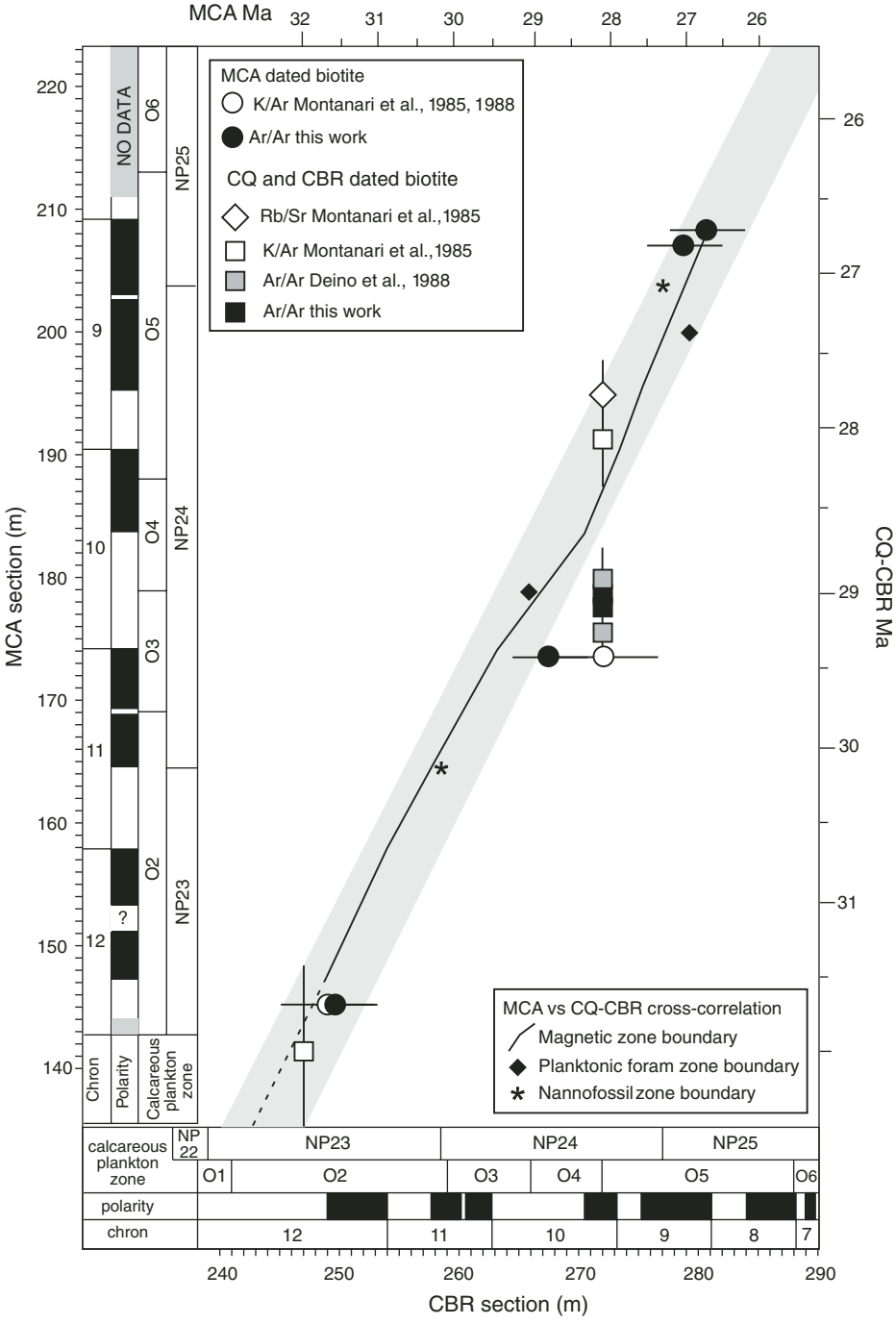

Figure 17. A geochronological synthesis based on a magnetostratigraphic cross-correlation between the Monte Cagnero (MCA) and the Contessa Quarry–Contessa Barbetti Road (CQ-CBR) sections

a strong effect of glacial event Oi-2a, located here at the boundary between Chronozone 10n and 9r. Coincidently, the $^{87}Sr/^{86}Sr$ curve from the Pieve d'Accinelli section exhibits a change in slope toward higher values starting within Chronozone 9r, which could be connected to a eustatic drop related to Oi-2a. (Fig. 7).

Volcaniclastic layers are found in all the well-calibrated sections (Figs. 5, 7, and 9), providing five radioisotopically dated levels within this time period. A geochronological synthesis based on a magnetostratigraphic cross-correlation between the Monte Cagnero and the Contessa Quarry–Contessa Barbetti Road section is shown in Figure 17. This magnetostratigraphic cross-correlation suggests a fairly linear accumulation rate throughout the Rupelian/Chattian boundary transition, but at Contessa the interval between the base of Chron 11r and the top of Chron 9n is about half as short as at Monte Cagnero, indicating a major difference in total accumulation rate between the two sections.

On the basis of the data shown in Figure 16, along with previous geochronologic results of Montanari et al. (1985, 1988; see Fig. 20), we conclude that within the Oligocene succession of the Umbria-Marche Apennines, there are only two stratigraphic levels to which we can confidently assign reliable numerical ages based on direct radioisotopic dating. At Monte Cagnero, the lower level is located at 145.6 m, in the lower third of Zone O2 of Berggren and Pearson (2005), which corresponds to the upper part of Chron 12r. Volcaniclastic biotite from this level yielded a replicated $^{40}Ar/^{39}Ar$ plateau age of 31.5 ± 0.2 Ma (2σ), consistent with a traditional K/Ar age of 31.7 ± 0.6 obtained by Montanari et al. (1985). The second level is located at 208 m in the same Monte Cagnero section, at the very top of Chron 9n. Four volcaniclastic biotite separates from this level yielded a mean $^{40}Ar/^{39}Ar$ plateau age of 26.7 ± 0.2 Ma, which is consistent with an astronomical age of 26.7 Ma for the top of Chron 9n obtained by Wade and Pälike (2004).

From these two tie points, a numerical age of 28.3 ± 0.2 Ma for the Rupelian/Chattian boundary, located in the upper half of Chron 10n at meter level 188 in the Monte Cagnero section, and corresponding to the O4/O5 planktonic foraminiferal zonal boundary, can be derived by simple interpolation, assuming constant accumulation rate throughout this stratigraphic interval. According to the astronomical timescale of Wade and Pälike (2004) and Pälike et al. (2005), and the paleomagnetic ages of Chron 10n provided by Gradstein et al. (2004), the age of the Rupelian/Chattian boundary would be 27.99 Ma and 28.36 Ma, respectively. The radioisotopìcally calibrated age of 28.3 ± 0.2 Ma for the

Rupelian/Chattian boundary provided by this study is very close to the ages of 28.426 Ma and 28.009 Ma proposed by Wade et al. (2007), and appears to be slightly younger than the age of 28.45 ± 0.1 Ma reported in recent chronostratigraphic and integrated magnetobiochronologic timescale compilations (e.g., Berggren et al., 1995; Gradstein et al., 2004; Luterbacher et al., 2004; Berggren and Pearson, 2005).

PROPOSAL

The integrated stratigraphic data presented in this work render the Monte Cagnero section the most representative for the Umbria-Marche Oligocene pelagic succession. This section bears continuous and complete biostratigraphic (calcareous plankton and dinoflagellate cysts), magnetostratigraphic, and chemostratigraphic records, and it is geochronologically calibrated with two reliable $^{40}Ar/^{39}Ar$ dates obtained from volcaniclastic biotite levels bracketing the Rupelian/Chattian boundary. The Monte Cagnero section meets the IUGS recommendations for a potential designation as a GSSP of the Rupelian/Chattian boundary (e.g., Odin and Montanari, 1988).

Following a multi-proxy approach, the reliable criteria for the definition of the Rupelian/Chattian boundary are: (1) the LCO of planktonic foraminifer *Chiloguembelina cubensis* that occurs within Chronozone 10n, (2) the LCO of calcareous nannofossil *Sphenolithus distentus* that consistently falls within Chronozone C9n.2n, (3) the *Svalbardella* abundance interval which is found within Chronozone 9n, (4) the base of Chronozone 10n, or (5) the carbon isotope peak related to Oi-2a, which is located at the top of Chronozone 10n. Given the apparently close association of criteria (1) and (5), we propose criteria (5) as the most useful and best potential for global correlation, but regardless of how the boundary is ultimately defined, the Monte Cagnero section of the Scaglia Cinerea records all of the above criteria and is thus an excellent choice for the GSSP for the Rupelian/Chattian stage boundary.

ACKNOWLEDGMENTS

We thank Mark Leckie and Kenneth G. Miller and for their useful comments and suggestions on the previous manuscript and also for encouraging us to resubmit this paper to the Geological Society of America Bulletin. We are grateful to Isabella Premoli Silva for reading the different versions of the manuscript and suggesting helpful ways in which it could be improved. We would like to thank the Cementerie Barbetti of Gubbio for kindly allowing us to work on the new Contessa Barbetti Road section; the Coldigioco Research Fund and the C.H. Potts Endowment Fund for supporting field and laboratory work of the Carleton College team; and Mike Jackson of the University of Minnesota Institute for Rock Magnetism for supervising the paleomagnetic analyses of the Pieve d'Accinelli section. We also thank Jim Zachos for giving us access to the University of California (UC) Santa Cruz Paleoclimate Laboratory for analyzing oxygen and carbon isotopes in our Pieve d'Accinelli samples; Sean McCauley for supervising Sr isotope analyses at UC Berkeley; and Tanya Atwater (UC Santa Barbara) for helping us collect core samples at Pieve d'Accinelli. The research for this paper was made possible by the financial support from the Cofin Ministero dell'Universitá e della Ricerca Scientifica e Tecnologica (MURST) 2003 (protocollo 2003041915-02) to S.M. and P.M. The Italian Council for Research (CNR) supported the R.C. (coordinator of the OLIS Working Group) with a grant (no. 97.00242.CT05). This is Publication no. 7 of the Centro di Geobiologia of the University of Urbino.

REFERENCES CITED

Baumann, P., and Roth, P.H., 1969, Zonierung des obereozans und Oligozaens des Monte Cagnero (Zentralapennin) mit planktonischen foraminiferen und nannoplankton: Eclogae Geologicae Helvetiae, v. 62, p. 303–323.

Berggren, W.A., 1971, Tertiary boundaries, *in* Funnel, B.F., and Riedel, W.R., eds., The micropalentology of the oceans: Cambridge, Cambridge University Press, p. 693–808.

Berggren, W.A., and Miller, K.G., 1988, Paleogene tropical planktonic foraminiferal biostratigraphy and magnetobiochronology: Micropaleontology, v. 34, p. 362–380, doi: 10.2307/1485604.

Berggren, W.A., and Pearson, P.N., 2005, A revised tropical to subtropical Paleogene planktonic foraminiferal zonation: Journal of Foraminiferal Research, v. 35, p. 279–298, doi: 10.2113/35.4.279.

Berggren, W.A., Kent, D.V., and Flynn, J.J., 1985, Paleogene geochronology and chronostratigraphy, *in* Snelling, N.J., ed., The chronology of the geological record: London, Geological Society of London Memoir, v. 10, p. 141–195.

Berggren, W.A., Kent, D.V., Swisher, C.C. III, and Aubry, M.-P., 1995, A revised Cenozoic geochronology and chronostratigraphy, *in* Berggren, W.A., Kent, D.V., Swisher, C.C. III, Aubry, M.-P., and Hardenbol, J., eds., Geochronology, time scales, and global stratigraphic correlation: SEPM (Society for Sedimentary Geology) Special Publication, v. 54, p. 129–212.

Blow, W.H., 1969, Late Middle Eocene to Recent planktonic foraminiferal biostratigraphy, *in* Bronnimann, P., and Renz, H.H., eds., Proceedings of the first international conference on planktonic microfossils (Geneva, 1967): Leiden, E.J. Brill, p. 199–421.

Bolli, H.M., and Saunders, J.B., 1985, Oligocene to Holocene low latitude planktic foraminifera, *in* Bolli, H.M., Saunders, J.B., and Perch-Nilsen, K., eds., Plankton stratigraphy: Cambridge, Cambridge University Press, p. 155–262.

Brinkhuis, H., and Biffi, U., 1993, Dinoflagellate cyst stratigraphy of the Eocene/Oligocene transition in central Italy: Marine Micropaleontology, v. 22, p. 131–183, doi: 10.1016/0377-8398(93)90007-K.

Brinkhuis, H., Powell, A.J., and Zevenboom, D., 1992, High-resolution dinoflagellate cyst stratigraphy of the Oligocene/Miocene transition interval in northwest and central Italy, *in* Head, M.J., and Wrenn, J.H., eds., Neogene and Quaternary dinoflagellat cyst and acritarchs: Dallas, American Association of Stratigraphic Palynologists Foundation, p. 219–258.

Cande, S.C., and Kent, D.V., 1992, A new geomagnetic polarity time scale for the Late Cretaceous and Cenozoic: Journal of Geophysical Research, v. 97, p. 13,917–13,951.

Cande, S.C., and Kent, D.V., 1995, Revised calibration of the geomagnetic polarity time scale for the Late Cretaceous and Cenozoic: Journal of Geophysical Research, v. 100, p. 6093–6095, doi: 10.1029/94JB03098.

Capo, R., and DePaolo, D.J., 1988, Sr isotopic analysis of marine carbonates from the Massignano section across the Eocene-Oligocene boundary, *in* Premoli Silva, I., Coccioni, R., and Montanari, A., eds., The Eocene-Oligocene boundary in the Marche-Umbria basin (Italy): Aniballi, Ancona, International Subcommission on Paleogene Stratigraphy, Special Publication, p. 189–192.

Capo, R., Montanari, A., and DePaolo, D.J., 1991, Flexure of the strontium isotopic curve in the upper Oligocene of the pelagic sequence at Gubbio: Signature of a major eustatic event?: Geological Society of America Abstracts with Programs, v. 23, p. 178.

Catanzariti, R., Rio, D., and Martelli, L., 1997, Late Eocene to Oligocene calcareous nannofossil biostratigraphy in northern Apennines: The Ranzano sandstone: Memorie Scienze Geologiche, v. 49, p. 207–253.

Deino, A., Channell, J., Coccioni, R., De Grandis, G., DePaolo, D.J., Emmanuel, L., Fornaciari, E., Laurenzi, M.L., Montanari, M., Renard, M., and Rio, D., 1997, Integrated stratigraphy of the upper Burdigalian-lower Langhian section at Moria (northeastern Apennines, Italy), *in* Montanari, A., Odin, G.S., and Coccioni, R., eds., Miocene stratigraphy: An integrated approach: Elsevier Science B.V. Developments in Paleontology and Stratigraphy, v. 15, p. 315–342.

de Kaenel, E., and Villa, G., 1996, Oligocene-Miocene calcareous nannofossil biostratigraphy and paleoecology from the Iberia Abyssal Plain, *in* Whitmarsh, R.B., Sawyer, D.S., Klaus, A., and Masson, D.G., eds., Proceedings of the Ocean Drilling Program: Scientific results, v. 149: College Station, Texas, Ocean Drilling Program, p. 79–145.

DePaolo, D.J., and Ingram, B.L., 1985, High-resolution stratigraphy with strontium isotopes: Science, v. 227, p. 938–941, doi: 10.1126/science.227.4689.938.

Fleck, R.J., Sutter, J.F., and Elliot, D.H., 1977, Interpretation of discordant $^{40}Ar/^{39}Ar$ age-spectra of Mesozoic tholeiites from Antarctica: Geochimica et Cosmochimica Acta, v. 41, p. 15–32, doi: 10.1016/0016-7037(77)90184-3.

Fornaciari, E., Raffi, I., Rio, D., Villa, G., Backman, J., and Olafsson, G., 1990, Quantitative distribution patterns of Oligocene and Miocene calcareous nannofossils from the western equatorial Indian Ocean, *in* Duncan, R.A., Backman, J., Peterson, L.C., et al., eds., Proceedings of the Ocean Drilling Program: Scientific results, v. 115: College Station, Texas, Ocean Drilling Program, p. 237–254.

Gradstein, F.M., Ogg, J.G., and Smith, A.G., 2004, A geologic time scale: Cambridge, Cambridge University Press, 589 p.

Hardenbol, J., and Berggren, W.A., 1978, A new Paleogene numerical time scale, *in* Cohee, G.V., Glaessner, M.F., and Hedberg, H.D., eds., The geologic time scale: Tulsa, American Association of Petroleum Geology, Studies in Geology, v. 6, p. 213–234.

Hardenbol, J., Thierry, J., Farley, M.B., Jacquin, T., de Graciansky, P.C., and Vail, P.R., 1998, Mesozoic and Cenozoic chronostratigraphic framework of European basins, *in* de Graciansky, P.C., Hardenbol, J., Jacquin, T., and Vail, P.R., eds., Mesozoic-Cenozoic sequence stratigraphy of European basins: Society of Sedimentary Geology, Special Publication, v. 60, p. 3–13.

Harland, W.B., Armstrong, R.L., Cox, A.V., Craig, L.E., Smith, A.G., and Smith, D.G., 1990, A geologic time scale 1989, revised edition: Cambridge, Cambridge University Press, 263 p.

Hess, J., Stott, L.D., Bender, M.L., Kennett, J.P., and Schilling, J.-G., 1989, The Oligocene marine microfossil record: Age assessments using strontium isotopes: Paleoceanography, v. 4, p. 655–679.

Husselmann, J., 1966, On the routine analysis of carbonates in unconsolidated sediments: Journal of Sedimentary Petrology, v. 36, p. 622–625.

Laskar, J., Robutel, P., Joutel, F., Gastineau, M., Correia, A., and Levrard, B., 2004, A long-term numerical solution for the insolation quantities of the Earth: Astronomy and Astrophysics, v. 428, p. 261–285, doi: 10.1051/0004-6361:20041335.

Leckie, R.M., Farnham, C., and Schmidt, M.G., 1993, Oligocene planktonic foraminifer biostratigraphy of Hole 803D (Ontong Java Plateau) and Hole 628A (Little Bahama Bank), and comparison with the southern high latitudes, *in* Berger, W.H., Kroenke, L.W., Mayer, L.A., et al., eds., Proceedings of the Ocean Drilling Program: Scientific results, v. 115: College Station, Texas, Ocean Drilling Program, p. 113–136.

Lo, C.H., and Onstott, T.C., 1989, ^{39}Ar recoil artifacts in chloritized biotite: Geochimica et Cosmochimica Acta, v. 53, p. 2697–2711, doi: 10.1016/0016-7037(89)90141-5.

Lo, C.H., Lee, J.K.W., and Onstott, T.C., 2000, Argon release mechanisms of biotite in vacuo and the role of short-circuit diffusion and recoil: Chemical Geology, v. 165, p. 135–165, doi: 10.1016/S0009-2541(99)00167-9.

Lowrie, W., 1997, Fundamentals of geophysics: Cambridge, Cambridge University Press, 368 p.

Lowrie, W., Alvarez, W., Napoleone, G., Perch-Nielsen, K., Premoli Silva, I., and Toumarkine, M., 1982, Paleogene magnetic stratigraphy in Umbrian pelagic carbonate rocks: The Contessa sections, Gubbio: Geological Society of America Bulletin, v. 93, p. 414–432, doi: 10.1130/0016-7606(1982)93<414:PMSIUP>2.0.CO;2.

Luterbacher, H.P., Ali, J.R., Brinkhuis, H., Gradstein, F.M., Hooker, J.J., Monechi, S., Ogg, J.G., Powell, J., Röhl, U., Sanfilippo, A., and Schmitz, B., 2004, The Paleogene period, *in* Gradstein, F.M., Ogg, J.G., and Smith, A.G., eds., A geologic time scale: Cambridge University Press, Cambridge, p. 384–408.

Maiorano, P., and Monechi, S., 2006, Early to Late Oligocene calcareous nannofossil bioevents in the Mediterranean (Umbria-Marche basin, central Italy): Rivista Italiana di Paleontologia e Stratigrafia. v. 12, p. 261–273.

Martini, E., 1971, Standard Tertiary and Quaternary calcareous nannoplankton zonation, *in* Farinacci, A., ed., Proceedings of the second planktonic conference, Rome 1970: Rome, Tecnoscienza, v. 2, p. 739–785.

Miller, K.G., Aubry, M.-P., Khan, M.J., Melillo, A.J., Kent, D.V., and Berggren, W.A., 1985, Oligocene-Miocene biostratigraphy of the western North Atlantic: Geology, v. 13, p. 257–261, doi: 10.1130/0091-7613(1985)13<257:OBMAIS>2.0.CO;2.

Miller, K.G., Wright, J.D., and Fairbanks, R.G., 1991, Unlocking the Ice House—Oligocene-Miocene oxygen isotopes, eustasy, and margin erosion: Journal of Geophysical Research, v. 96, B4, p. 6829–6848.

Miller, K.G., Kominz, M.A., Browning, J.V., Wright, J.D., Mountain, G.S., Katz, M.E., Sugarman, P.J., Cramer, B.S., Christie-Blick, N., and Pekar, S.F., 2005, The Phanerozoic record of global sea-level change: Science, v. 310, p. 1293–1298, doi: 10.1126/science.1116412.

Min, K., Renne, P.R., and Huff, W.D., 2001, ^{40}Ar/^{39}Ar dating of Ordovician K-bentonites in Laurentia and Baltoscandia: Earth and Planetary Science Letters, v. 185, p. 121–134, doi: 10.1016/S0012-821X(00)00365-4.

Montanari, A., and Koeberl, C., 2000, Impact stratigraphy—The Italian record: Lecture Notes in Earth Sciences, v. 93, 364 p.

Montanari, A., Drake, R., Bice, D.M., Alvarez, W., Curtis, G.H., Turrin, B.T., and DePaolo, D.J., 1985, Radiometric time scale for the upper Eocene and Oligocene based on K-Ar and Rb-Sr dating of volcanic biotites from the pelagic sequence of Gubbio, Italy: Geology, v. 13, p. 596–599, doi: 10.1130/0091-7613(1985)13<596:RTSFTU>2.0.CO;2.

Montanari, A., Deino, A., Drake, R., Turrin, B.T., DePaolo, D.J., Odin, G., Curtis, G.H., Alvarez, W., and Bice, D.M., 1988, Radioisotopic dating of the Eocene/Oligocene boundary in the pelagic sequence of the northern Appenines, *in* Premoli Silva, I., Coccioni, R., and Montanari, A., eds., The Eocene-Oligocene boundary in the Marche-Umbria basin (Italy): Aniballi, Ancona, International Subcommission on Paleogene Stratigraphy, Special Publication, p. 195–208.

Montanari, A., Deino, A., Coccioni, R., Langenheim, V.E., Capo, R., and Monechi, S., 1991, Geochronology, Sr isotope analysis, magnetostratigraphy, and planktonic stratigraphy across the Oligocene-Miocene boundary in the Contessa section (Gubbio, Italy): Newsletters in Stratigraphy, v. 23, p. 151–180.

Montanari, A., Bice, D.M., Capo, R., Coccioni, R., Deino, A., DePaolo, D.J., Emmanuel, L., Monecchi, S., Renard, M., and Zevenboon, D., 1997a, Integrated stratigraphy of the Chattian to mid-Burdigalian pelagic sequence of the Contessa valley (Gubbio, Italy), *in* Montanari, A., Odin, G.S., and Coccioni, R., eds., Miocene stratigraphy—An integrated approach: Developments in Palaeontology and Stratigraphy, Elsevier, v. 15, p. 249–277.

Montanari, A., Beaudoin, B., Chan, L.S., Coccioni, R., Deino, A., DePaolo, D.J., Emmanuel, L., Fornaciari, E., Kruge, M., Lundblad, S., Mozzato, C., Portier, E., Renard, M., Rio, D., Sandroni, P., and Stankiewicz, A., 1997b, Integrated stratigraphy of the Middle to Upper Miocene pelagic sequence of the Cònero Riviera (Marche region, Italy), *in* Montanari, A., Odin, G.S., and Coccioni, R., eds., Miocene stratigraphy—An integrated approach: Developments in Palaeontology and Stratigraphy, Elsevier, v. 15, p. 409–450.

Nocchi, M., Parisi, G., Monaco, P., Monechi, S., and Madile, M., 1988, Eocene and Early Oligocene micropaleontology and paleoenvironments in SE Umbria, Italy: Palaeogeography, Palaeoclimatology, Palaeoecology, v. 67, p. 181–244, doi: 10.1016/0031-0182(88)90154-X.

Odin, G.S., and Montanari, A., 1988, The Eocene-Oligocene boundary at Massignano (Ancona, Italy): A potential boundary stratotype, *in* Premoli Silva, I., Coccioni, R., and Montanari, A., eds., The Eocene-Oligocene boundary in the Marche-Umbria basin (Italy): Aniballi, Ancona, International Subcommission on Paleogene Stratigraphy, Special Publication, p. 253–263.

Okada, H., and Bukry, D., 1980, Supplementary modification and introduction of code numbers to the low-latitude coccolith biostratigraphic zonation (Bukry, 1973; 1975): Marine Micropaleontology, v. 5, p. 321–325, doi: 10.1016/0377-8398(80)90016-X.

Olafsson, G., and Villa, G., 1992, Reliability of sphenoliths as zonal markers in Oligocene sediments from the Atlantic and Indian Oceans: Memorie di Scienze Geologiche, v. 43, p. 261–275.

Pälike, H., Moore, T., Backman, J., Raffi, I., Lanci, L., Parés, J.M., and Janecek, T., 2005, Integrated stratigraphic correlation and improved composite depth scales for ODP Sites 1218 and 1219, *in* Wilson, P.A., Lyle, M., and Firth, J.V., eds., Proceedings of the Ocean Drilling Program: Scientific results, v. 199: College Station, Texas, Ocean Drilling Program, p. 1–41.

Parisi, G., Guerrera, F., Madile, M., Magnoni, G., Monaco, P., Monechi, S., and Nocchi, M., 1988, Middle Eocene to early Oligocene calcareous nannofossil and foraminiferal biostratigraphy in the Monte Cagnero section, Piobbico (Italy), *in* Premoli Silva, I., Coccioni, R., and Montanari, A., eds., The Eocene-Oligocene boundary in the Marche-Umbria basin (Italy): Aniballi, Ancona, International Subcommission on Paleogene Stratigraphy, Special Publication, p. 119–135.

Pekar, S.F., DeConto, R.M., and Harwood, D.M., 2006, Resolving a late Oligocene conundrum: Deep-sea warming and Antarctic glaciation: Palaeogeography, Palaeoclimatology, Palaeoecology, v. 231, p. 29–40, doi: 10.1016/j.palaeo.2005.07.024.

Poore, R.Z., 1984, Middle Eocene through Quaternary planktonic foraminifers from the southern Angola Basin: Deep Sea Drilling Project Leg 73, *in* Hsü, K.J., LaBrecque, J.L., et al., eds., Initial reports of the Deep Sea Drilling Project, v. 73: Washington, D.C., U.S. Government Printing Office, p. 429–448.

Poore, R.Z., Tauxe, L., Percival, S.F., Jr., and LaBrecque, J.L., 1982, Late Eocene-Oligocene magnetostratigraphy and biostratigraphy at South Atlantic DSDP site 522: Geology, v. 10, p. 508–511, doi: 10.1130/0091-7613(1982)10<508:LEMABA>2.0.CO;2.

Premoli Silva, I., and Jenkins, D.G., 1993, Decision on the Eocene-Oligocene boundary stratotype: Episodes, v. 16, p. 379–382.

Pujol, C., 1983, Cenozoic Planktonic foraminiferal biostratigraphy of the Southwestern Atlantic (Rio Grande Rise): Deep Sea Drilling Project Leg 72, *in* Barker, P.F., Johnson, D.A., et al., eds., Initial reports of the Deep Sea Drilling Project, v. 72: Washington, D.C., U.S. Government Printing Office, p. 623–673.

Reilly, T.J., Miller, K.G., and Feigenson, M.D., 2002, Latest Eocene–earliest Miocene Sr isotopic reference section, Site 522, eastern South Atlantic: Paleoceanography, v. 17, no. 3, p. 1046–1055, doi: 10.1029/2001PA000745.

Roth, P.H., 1970, Oligocene Calcareous nannoplankton biostratigraphy: Eclogae Geologicae Helvetiae, v. 63, p. 799–881.

Roth, P.H., 1983, Jurassic and Lower Cretaceous calcareous nannofossils in the western North Atlantic (Site 534): Biostratigraphy, preservation and some observation on biogeography and paleoceanography: Initial Reports of the Deep Sea Drilling Project, v. 76, p. 587–621.

Roth, P.H., and Thierstein, H., 1972, Calcareous nannoplankton: Leg 14 of the Deep Sea Drilling Project: Initial Reports of the Deep Sea Drilling Project, v. 14, p. 421–485.

Schlanger, S.O., and Premoli Silva, I., 1986, Oligocene sea-level falls recorded in mid-Pacific atoll and archipelagic apron settings: Geology, v. 14, p. 392–395, doi: 10.1130/0091-7613(1986)14<392:OSFRIM>2.0.CO;2.

Spezzaferri, S., 1994, Planktonic foraminiferal biostratigraphy and taxonomy of the Oligocene and lower Miocene in the oceanic record: An overview: Paleontographia Italica, v. 81, 187 p.

Spezzaferri, S., 1998, Planktonic foraminifer biostratigraphy and paleoenvironmental implications of Leg 152 Sites (East Greenland Margin), *in* Saunders, A.D., Larsen, H.C., and Wise, S.W. Jr., eds., Proceedings of the Ocean Drilling Program: Scientific results, v. 152: College Station, Texas, Ocean Drilling Program, p. 161–189.

Van Simaeys, S., De Man, E., Vandenberghe, N., Brinkhuis, H., and Steurbaut, E., 2004, Stratigraphic and palaeoenvironmental analysis of the Rupelian-Chattian transition in the type region: Evidence from dinoflagellate cysts, foraminifera and calcareous nannofossils: Palaeogeography, Palaeoclimatology, Palaeoecology, v. 208, p. 31–58, doi: 10.1016/j.palaeo.2004.02.029.

Van Simaeys, S., Brinkhuis, H., Pross, J., Williams, G.L., and Zachos, J.C., 2005, Arctic dinoflagellate migrations mark the strongest Oligocene glaciations: Geology, v. 33, p. 709–712, doi: 10.1130/G21634.1.

Vonhof, H.B., Smit, J., Brinkhuis, H., and Montanari, A., 1998, Late Eocene impacts accelerated global cooling?, *in* Vonhof, H.B., The Strontium stratigraphic record of selected geologic events [Ph.D. Thesis]: Utrecht, University of Utrecht, p. 77–90.

Wade, B.S., and Pälike, H., 2004, Oligocene climate dynamics: Paleoceanography, v. 19, p. PA4019, doi: 10.1029/2004PA001042

Wade, B.S., Berggren, W.A., and Olsson, R.K., 2007, The biostratigraphy and paleobiology of Oligocene planktonic foraminifera from the equatorial Pacific Ocean (ODP Site 1218): Marine Micropaleontology, v. 62, p. 167–179, doi: 10.1016/j.marmicro.2006.08.005.

Williams, G.L., Fensome, R.A., and Lentin, J.K., 1998, The Lentin and Williams index of fossil dinoflagellates, 1998 edition: American Association of Stratigraphic Palynologists Foundation, Contribution Series, v. 34, 817 p.

Wilpshaar, M., Santarelli, A., Brinkhuis, H., and Visscher, H., 1996, Dinoflagellate cysts and mid-Oligocene chronostratigraphy in the central Mediterranean region: Journal of the Geological Society, v. 153, p. 553–561.

Zachos, J.M., Pagani, M., Sloan, L., Thomas, E., and Billups, K., 2001, Trends, rhythms, and aberrations in global climate 65 Ma to present: Science, v. 292, p. 686–693, doi: 10.1126/science.1059412.

Manuscript received 15 February 2007
Revised manuscript received 11 July 2007
Manuscript accepted 17 July 2007

Printed in the USA